Structure-Function Relationship of The Sterol Transporter ABCG5/G8: Expression, Purification and Enzymatic Characterization of ABCG5/G8 Missense Loss of Function Mutations.

Aiman Zein

Thesis submitted to the University of Ottawa
in partial Fulfillment of the requirements for the
Master of Science Biochemistry

Department of Biochemistry, Microbiology and Immunology
Faculty of Medicine
University of Ottawa

Abstract

The heterodimeric ATP-binding cassette (ABC) transporter, ABCG5/G8, is responsible for direct secretion of cholesterol and dietary sterols into the gut lumen and the bile. Inactivating mutations of ABCG5/G8 cause sitosterolemia, a rare autosomal recessive disease characterized by the accumulation of plant sterols in plasma, hypercholesterolemia and development of premature coronary heart disease. Functional and structural characterization of ABCG5/G8 is necessary to understand its mechanism and how the genetic defects impact its function. In this thesis, I expressed seventeen constructs of various disease-causing or catalytically deficient missense mutations in *Pichia pastoris* yeast. This establishes reagents for *in vitro* functional and structural studies. Secondly, I focused on two disease mutants (ABCG5-E146Q and ABCG8-R543S) and a sterol binding mutation (ABCG5-A540F) and established large-scale purification of these mutants. Using a cholesterol hemisuccinate (CHS)-dependent ATPase assay, I determined ATP hydrolysis by these three mutants and analyze their kinetic parameters. All missense mutants showed a significantly impaired ATPase activity, but the ability of ATP binding appeared unchanged between the WT and the mutants. This work demonstrates an intimate structure-function relationship in ABCG5/G8 and sheds some light on the mechanistic details of this important cholesterol-regulating ABC transporter.

ACKNOWLEDGMENTS

I would like to extend my gratitude to my supervisor Professor Jyh-Yeuan Lee for his excellent guidance and his everlasting patience. I sincerely thank my committee members, Dr. John Baenziger and Dr. Jean-Francois Couture who have provided me with very helpful suggestions and insightful feedbacks and encouragement over the last two years. A very special thanks all the members of the Lee lab for invaluable advice and indefinite help specially Dr. Bala Xavier, William Jennings (Bill) and Angelica Venes.

Finally, and most importantly, I would like to thank my wife and my two little kids, Hadi and Haya, for their patience and support during my graduate study.

Table of Contents

ABREVIATIONS

A

ABC – ATP binding cassette

ACAT2 - acetyl-CoA acetyltransferase 2

ADP – Adenosine diphosphate

ATP – Adenosine triphosphate

ApoAI - apolipoprotein A-I

B

BSA – Bovine serum albumin

C

CBP - calmodulin binding peptide

CD – Circular dichroism

CHS - cholesteryl hemisuccinate

CMC – Critical micelle concentration

D

DEAE - Diethylaminoethyl

DDM – n- Dodecyl β D- maltoside

DMSO – Dimethyl sulphoxide

DNA – Deoxy ribonucleic acid

DTT – Dithiotheritol

E

E. coli – Escherichia coli

EDTA – Ethylene diamino tetraacetic acid

EGTA - ethylene glycol-bis (β-aminoethyl ether)-N,N,N′,N′-tetraacetic acid

ER – Endoplasmic reticulum

F

FGF - fibroblast growth factor

FXR - farnesoid-X receptor

G

GFP – Green fluorescence protein

H

HDL- high-density lipoproteins

His – Histidine

HMG-CoA - 3-hydroxy-3-methyl-glutaryl-coenzyme A

HNF4α- hepatocyte nuclear factor 4 alpha

K

K_M – Michaelis-Menton constant

L

LB- Luria-Bertani

LDL- low-density lipoproteins

LRH-1 - liver receptor homolog-1

LXR- liver-X receptor

M

MβCD - Methyl-β-cyclodextrin

MDR- multidrug resistance

MGY- minimal glycerol yeast nitrogen base

N

Ni-NTA - nickel-nitrilotriacetic acid

NPC1L1 - Niemann-Pick C1-Like 1

NBD – Nucleotide binding domain

NF-κB - kappa-light-chain-enhancer of active B cells

P

P. pastoris – Pichia pastoris

PAGE – Polyacrylamide gel electrophoresis

PCR – Polymerase chain reaction

PCSK9- Proprotein convertase subtilisin/kexin type 9

PAOX1 - powerful methanol-regulated alcohol oxidase promoter

Pi – Inorganic phosphate

PVDF - Polyvinylidene fluoride

PM – Plasma membrane

R

RCT - reverse cholesterol transport

RNA – Ribonucleic acid

RT – Room temperature

S

SDS – Sodium dodecyl sulphate

SEC – Size exclusion chromatography

SMA – Styrene maleic acid

SMALP – Styrene maleic acid lipid particle

T

TICE - transintestinal cholesterol efflux

TMD - transmembrane domains

TCEP - Tris (2-carboxylethyl) phosphine

TBST- Tris-Buffered Saline, 0.1% Tween

Y

YNB – Yeast nitrogen base

YPD – Yeast peptone dextrose

LIST OF FIGURES

LIST OF TABLES

Chapter I Introduction

1.1 Cholesterol Homeostasis and Hyperlipemia

Cholesterol, a key component of cellular membranes, is required for synthesis of steroid hormones and bile acids, thus playing a vital role in cellular function and survival (Yang et al., 2016). Cholesterol has been shown to increase the rigidity of phospholipid-based lipid bilayer, which is regulated by the permeability and flexibility of cell membranes (Harayama et al., 2018). Additionally, cholesterol is an essential component of the lipid microdomains (also known as Rafts), which are involved in a wide range of biological processes including signaling events (Simons et al., 1997). Dysregulation of cholesterol metabolism is a hallmark of cardiovascular and metabolic disorders, including atherosclerosis and fatty liver disease (Tall et al., 2008). Globally, cardiovascular diseases account for ~50% deaths of non-communicable diseases (Bloom et al., 2011). Abnormal elevation of plasma cholesterol is thus considered a key biomarker in the development of these disorders (Nelson et al., 2013).

In vertebrates, cholesterol is obtained from the diet or by *de novo* biosynthesis from acetyl-CoA (van der Velde et al., 2010). To maintain cholesterol balance, an equivalent amount of cholesterol must be eliminated from cells and tissues. Circulating high-density lipoprotein (HDL) and low-density lipoprotein (LDL) particles serve as conduits for the transport of cholesterol and other lipids

between tissues. Elevations in the levels of LDL and reductions in the levels of HDL result in accumulation of cholesterol on the walls of arteries, which can initiate the development of atherosclerosis (Brown et al. 1981). Currently, the *de novo* biosynthesis pathway of cholesterol is the major target of interventions aimed at controlling cholesterol level in the body. This is achieved either by statin treatment that inhibits the HMG-CoA reductase or by using anti-PCSK9 monoclonal antibodies to promote uptake of LDL through cell-surface LDL receptors (LDLRs). Unfortunately, many patients are resistant to statin treatment or develop side effects, and the current antibody treatment modalities are not cost-effective (Reiner 2014). Moreover, it has been extremely challenging to target HDL metabolism, and several clinical trials have already failed. For example, attempts to boost cholesterol efflux by liver-X receptor (LXR) agonists led to severe side effects, such as steatosis (abnormal retention of lipids) (Kirchgessner et al., 2006). Ezetimibe is another drug that was found to reduce the absorption of dietary cholesterol but not effectively (Phan et al., 2012). There is thus an urgent need of alternative therapies to manage elevated cholesterol and its associated symptoms.

Few cells have the capacity to metabolize cholesterol, and thus its elimination through biliary and intestinal secretion is critical to maintain whole body cholesterol level. Whether derived from the diet or *de novo* synthesis, sterols in peripheral tissues are mobilized to HDL and ultimately delivered to the liver or intestine for elimination by the reverse cholesterol transport (RCT) pathway

(Ohashi et al., 2005). While elimination of excess cholesterol is vital for life, little is known about the mechanisms underlying the control of sterol shuttling across lipid-bilayer membranes. RCT is a process that accelerates cholesterol transportation from either the peripheral tissues or macrophages to HDL particles in the plasma or through the hepatobiliary or transintestinal cholesterol secretion into the gut lumen (van der Velde et al., 2010). In the plasma, apolipoprotein A-I (ApoAI) and phospholipids form nascent HDL that can accept and carry away cholesterol from cells, such the basal hepatocytes or circulating macrophages. This cholesterol transport process is believed to be initially facilitated by the membrane-spanning cholesterol-transport ABCA1, an ATP-binding cassette (ABC) protein (Tall et al., 2008). ABCG1, another ABC cholesterol transporter, then stimulates maturation of HDL that transports the cholesterol to other tissues for further usage.

The majority of cholesterol is then eliminated from the body through biliary secretion, either as free cholesterol or following its metabolism to bile acids in the liver (Tall et al., 2008; Patel et al., 1998). This is considered the final step of RCT and is largely mediated by the heterodimeric sterol transporter ABCG5/G8, which accounts for more than 75% of biliary cholesterol secretion (Yu et al., 2002). Using animal models, the hepatic expression of ABCG5/G8 transgenes increased biliary cholesterol secretion and was protective against the development of atherosclerotic plaques (Yu et al., 2002), whereas accelerating RCT was shown to counteract the development of atherosclerosis (Yu et al., 2002).Together with the

discovery of different ABC transporters on the apical membranes of hepatocytes and enterocytes, this final step of RCT has recently gained increasing interest in the effort to control secretion of cholesterol and phospholipids into bile (Ouimet et al., 2019). However, no clinically approved therapeutics are available to accelerate RCT yet; and thus, deciphering the mechanisms that regulate RCT and uncovering novel targets that can accelerate this pathway are of utmost significance.

1.2 Sitosterolemia

Over 90 years ago, dietary cholesterol was found to be a key part of cholesterol hemostasis (Schoenheimer et al., 1929). Despite its *de novo* synthesis and excretion via the hepatobiliary system, the small intestines selectively absorb dietary cholesterol and exclude other non-cholesterol sterols (xenosterols), including phytosterols (Patel et al., 1998). In 1974, Bhattacharyya and Connor reported differential absorption of dietary sterols and described a disease, namely sitosterolemia, which affected two sisters with high levels of plant sterols in their plasma (Bhattacharyya et al., 1974). The disease is a rare autosomal recessive human disorder, caused by mutations in either of two genes, *ABCG5* or *ABCG8*, on human chromosome 2p21 (Patel et al., 1998). These genes encode for two ABC transporter proteins, ABCG5 and ABCG8, that, are exclusively expressed in the liver and the small intestines (Graf et al., 2003). They function by forming a

heterodimeric complex, ABCG5/G8, and then promoting sterol efflux into the bile and small intestines (Yu et al., 2002). Patients with inactivating mutations in either ABCG5 or ABCG8 develop sitosterolemia, causing accumulation of plant sterols in plasma, premature coronary heart disease and hypercholesterolemia (Kidambi et al., 2008). The phenotype of sitosterolemia can be recapitulated with genetically modified mice lacking functional ABCG5/G8 (Abcg5/g8$^{-/-}$), showing massively increased (>30-fold) absorption of plant sterols in these animals, as well as elevated hepatic and plasma cholesterol (Yu et al., 2002).

1.3 ATP-Binding Cassette (ABC) Transporters

ABC transporters are found in all organisms, from bacteria to eukaryotes (Dean et al., 1995). Most eukaryotic ABC transporters work as exporters, whereas in prokaryotes, they function as both exporters and importers (Dean et al., 1995). Utilizing the energy released from the binding and hydrolysis of ATP, they control the movement of a variety of solutes such as sugars, amino acids, peptides, ions and a wide range of hydrophobic compounds across cell membranes (Wilkens 2015). In humans, there are 44 ABC transporters, divided into 5 subfamilies known as ABCA, B, C, D and G (Xavier et al., 2019). These transporters play important physiological roles in different human tissues, and malfunctions of several members have been implicated in many diseases (Xavier et al., 2019). All ABC

transporters share a common topological architecture, which includes two nucleotide binding domains (NBDs) and two transmembrane domains (TMDs). Some ABC transporters are made up of a single TMD and a single NBD (also known as half transporters); and usually need to form a homo- or hetero-dimer in order to be functional (Higgins 1992).

NBDs of ABC transporters are characterized by the presence of highly conserved Walker A, Walker B and ABC signature motifs, and it is believed that the mechanism of ATP catalysis in the NBDs may be common across all ABC transporters. The NBDs are positioned in the cytoplasm and carry out the ATPase activity, which provides the energy needed for substrate translocation across the membrane (Ford et al., 2019). In general, NBDs dimerize during the transport cycle, create an interface that allows the binding and hydrolysis of ATP, and thereby generate the power stroke to drive active transport of substrates across biological membranes. On the other hand, TMDs of ABC transporters have been shown to have low similarities in sequence, as well as 3-D structural folds, suggesting distinct mechanisms for unique transport substrates (Holland et al., 1999; Thomas et al., 2018; Ford et al., 2019).

My thesis research project focused on ABCG5 and ABCG8, two of five subfamily-G ABC (ABCG) transporters in humans (Holland 2011). ABCG proteins are half transporters with each containing one N-terminal NBD and one C-terminal TMD, and homo- or hetero-dimerization is therefore needed for functional and

active transporters (Woodward et al., 2011). ABCG1, ABCG4, ABCG5 and ABCG8 are associated with lipid and/or cholesterol metabolism, while ABCG2 carries out drug efflux and transports uric acids (Xavier et al., 2018). ABCG2 is expressed in various tissues and can contribute to multidrug resistance (MDR) in cancer chemotherapy. ABCG1 and ABCG4 play important roles in maintaining the cholesterol balance in the brain and macrophage-rich tissues (Zoltán et al., 2016). ABCG5 and ABCG8, exclusively expressed in the small intestine and the liver, heterodimerize to efflux cholesterol into bile and gut lumen (Graf et al., 2003).

1.4 Regulation and Function of ABCG5/G8 Sterol Transporter

ABCG5 and ABCG8 are two ABC proteins encoded by two independent genes that are positioned head-to-head on opposite strands and separated by only 374 base pairs (Berge et al., 2000). Their proximity and opposite orientation suggest that these genes share a common, bidirectional promoter and regulatory elements. Several transcription factors are known to regulate ABCG5/G8, including hepatocyte nuclear factor 4 alpha (HNF4α), GATA4, and GATA6 (Sumi et al., 2007). In addition, binding of liver receptor homolog-1 (LRH-1) was mapped to be between 134 to 142 nucleotides of this intergenic region (Freeman et al., 2004). While no specific response elements have been identified for the farnesoid-X receptor (FXR/NR1H4), FXR has been shown to

transcriptionally control ABCG5/G8 via bile acid signaling (Wang et al., 2006). Previous studies showed that administration of cholic acids in mice could enhance transcription of ABCG5 and ABCG8 (Kamisako et al., 2007), and this was shown to be FXR-dependent and partially mediated by fibroblast growth factor 15/19 (FGF15/19) and/or inhibition of nuclear factor kappa-light-chain-enhancer of active B cells (NF-κB) (Balasubramaniyan et al., 2016). Furthermore, the response elements of liver-X receptors (LXRα and LXRβ) were mapped on both genes (Byun et al., 2019).

Post-translational modification is necessary for proper maturation of functional ABCG5/G8 heterodimers, of particular N-glycosylation that enables protein folding and escaping the endoplasmic reticulum (ER) (Graf et al., 2002). Both subunits are N-glycosylated on their extracellular domains, where ABCG5 is glycosylated at two sites (Asn585 and Asn592) and ABCG8 is glycosylated at one site (Asn619). Studies using mammalian cell models confirmed that glycosylation on ABCG8 is the minimal requirement to escape ER, and glycosylation of ABCG5 can facilitate the trafficking of the heterodimers to the cell surface (Graf et al., 2004).

ABCG5/G8 is the primary cholesterol transporter from hepatocytes to bile, accounting for more than 70% of the total biliary secretion (Yu et al., 2005). The elimination of cholesterol through ABCG5/G8 requires the formation of bile micelles, a process that is facilitated in conjunction with other ABC transporters on

the bile duct and in the canalicular membrane of hepatocytes, including bile salt transporter ABCB11 and phospholipid transporter ABCB4 (Shuguang et al., 2014). In addition, ABCG5/G8 redirects the absorption of cholesterol and phytosterols in the small intestine (Yu et al., 2005). Recent studies have shown that ABCG5/G8 is the primary sterol transporter responsible for the elimination of dietary neutral sterols through transintestinal cholesterol efflux (TICE) (Grefhorst et al., 2019).

Dietary cholesterol and plant sterols are obtained from daily diet. It is believed that upon digestion, they are incorporated in micelles and transported to a close contact to Niemann-Pick C1-Like 1 (NPC1L1) on the brush border membrane of the small intestine (Figure 1.1). Presence of NPC1L1 plays an important role in the absorption of sterols from micelles in the lumen of the small intestine, a step that is believed to be blocked by the drug ezetimibe in enterocytes (Jakulj et al., 2016). What remains unclear is whether ABCG5/G8 has direct selectivity between cholesterol and plant sterols. Less than 5% of dietary plant sterols are normally absorbed, although sitosterolemia patients can accumulate up to 100-fold higher plant sterols than healthy individuals (Berge et al., 2000) The ABCG5/G8-deficient mice have shown higher accumulation of plasma plant sterols, nearly 300-fold increase, and the WT animals secrete plant sterols into the bile at higher rates than cholesterol (Michael et al., 2003). In enterocytes, cholesterol is selectively esterified by acetyl-CoA acetyltransferase 2 (ACAT2), which provides a mean of differential absorption of sterols (Nguyen et al., 2012).

However, the contribution of such ACAT2-depedent selectivity (<10-fold difference) is not enough to account for a much higher accumulation of plant sterols in patients or in model animals. It thus appears that ABCG5/G8 would play a critical role in sterol transport selectivity, but a direct evidence from *in vitro* analyses remains to be determined.

The difference in chemical structures of sterols may play a very important role in the ABCG5/G8-mediated transport specificity. Compared to cholesterol, all phytosterols have the same identical steroid-ring structure, but they differ by an additional group on their carbon number 24 (C24). Figure 1.2 shows the chemical structures of five sterols. Campesterol has an additional methyl group at C24, while β-sitosterol and stigmasterol have an ethyl group instead and stigmasterol also has a double bond between carbon 22 and 23. Using transgenic mice, *in vivo* studies have suggested that the alkylation of the C24 might affect the specificity of ABCG5/G8 to different sterols (Yu et al., 2004). For example, deficiency of ABCG5/G8 led to a more significant increase of stigmasterol than cholesterol, suggesting that sterols with such ethyl group at C24 and double bond between carbon 22 and 23 may be a more preferable substrate than cholesterol.

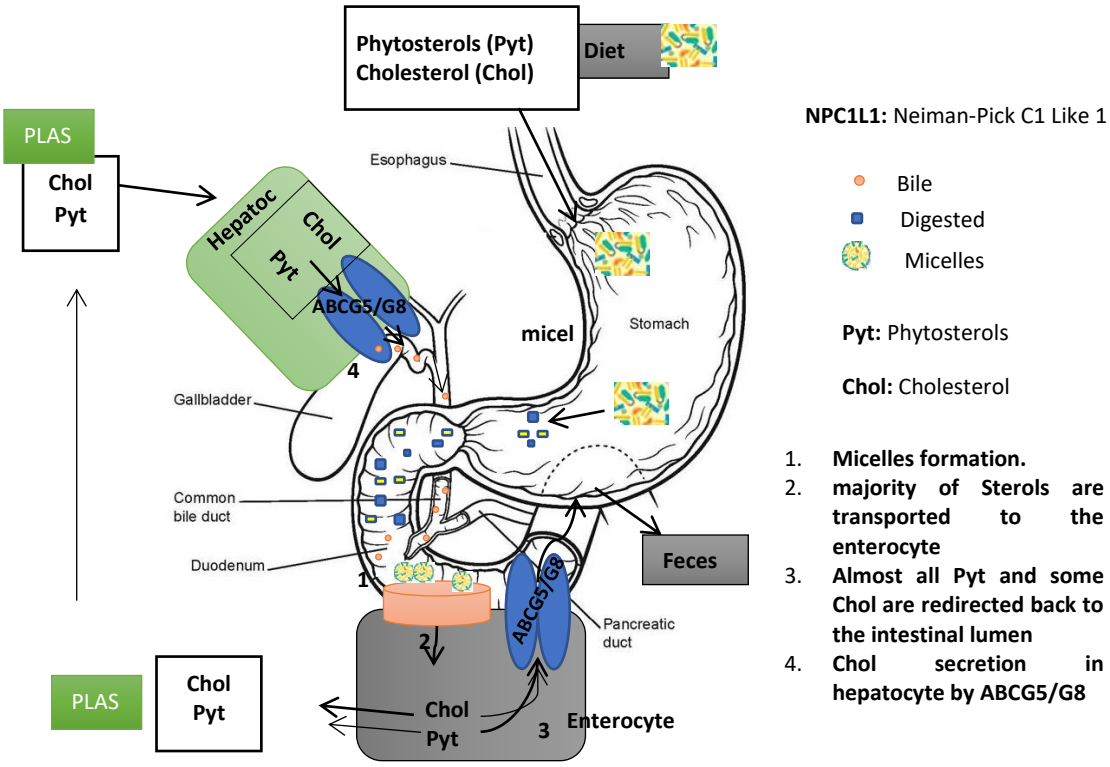

Figure 1. 1: Absorption and secretion of cholesterol (Chol) and phytosterols (Pyt).

1: Dietary sterols form micelles within the intestinal lumen along with other digested lipids. **2**: Micelles are transported to the brush border where the majority of the chol and pyt will be transported to the enterocyte by specific transporter Neiman-Pick C1 Like 1 (NPC1L1). **3**: However, nearly all of the Pyt and some chol are redirected back to the intestinal lumen by the transporters ATP binding cassette (ABC) transporter G5/G8 (ABCG5/G8) for excretion from the body. About half of the cholesterol is packaged into lipoproteins and transported into the bloodstream for delivery to the liver. **4:** cholesterol secretion in the hepatocytes is mediated by ABCG5/G8.

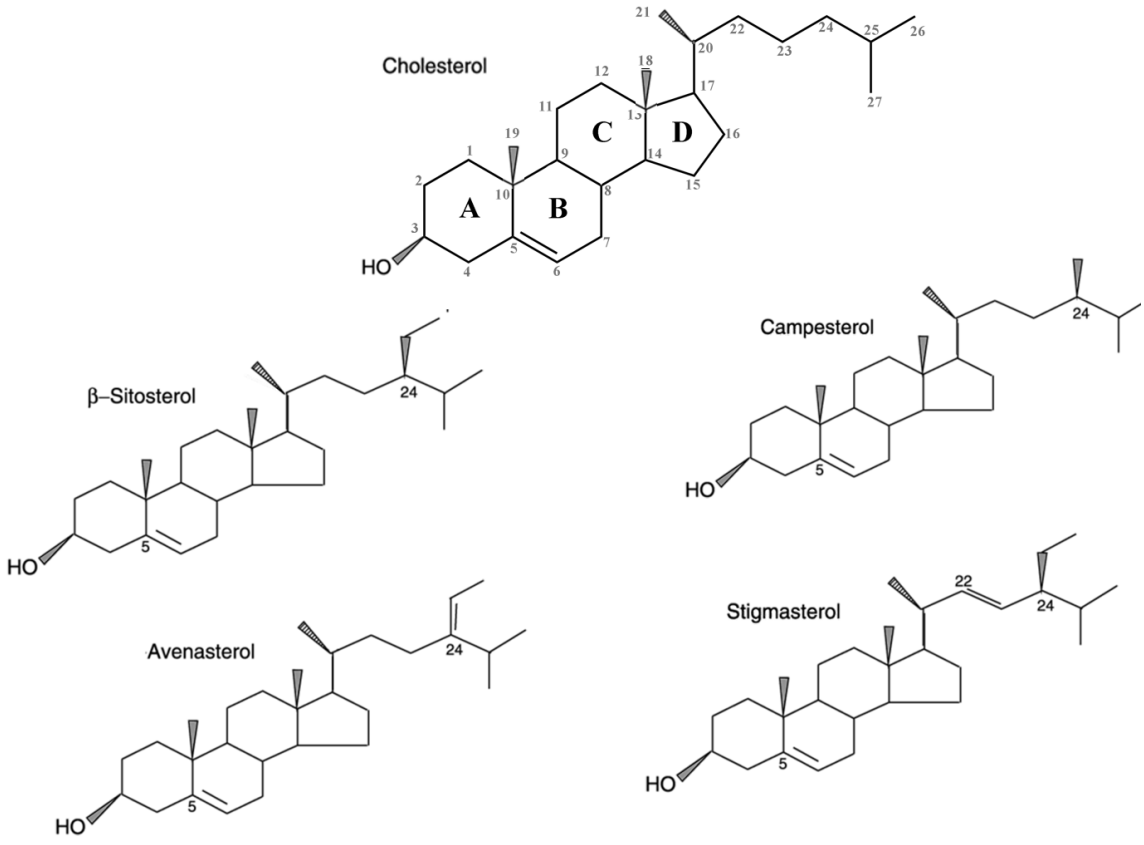

Figure 1. 2: Sterol structures of cholesterol and four phytosterols (plant sterols).

These sterols show a same identical ring structure with major difference a different alkyl group at Carbon 24 with an addition double bond on stigmasterol between carbon 22 and 23.

1.5 Protein Biosynthesis of the ABCG5/G8 Disease-causing Mutants

ABCG5 and ABCG8 are glycoproteins which are required to form a heterodimer for proper folding and functional expression on the cell surface. Although glycosylation was previously shown not to be required for heterodimerization of ABCG5 and ABCG8, either subunit is able to traffic efficiently out of the ER if at least an *N*-linked glycan is present on ABCG8 (Graf et al., 2004). Using the characteristics and the role of *N*-linked glycans in dimer formation and trafficking of the ABCG5/G8 transporter, protein maturations of 13 disease-causing missense mutations in either ABCG5 or ABCG8 were compromised to various degrees (Graf et al., 2004). Most mutations result in protein retention in the ER, which prevented efficient trafficking to the Golgi apparatus and cell surface. However, five disease mutants matured and underwent proper N-glycosylation, albeit to a lower expression level when compared to the wild-type protein (Graf et al., 2004). In this thesis, I have exploited such characteristics of protein maturation for mutant cloning and protein engineering.

1.6 Crystal Structure of Human ABCG5/G8

ABCG5 and ABCG8 share relatively low sequence identity (~28% identity in their amino acid sequences). Using X-ray crystallography, an atomic model of the human ABCG5/G8 was resolved in phospholipid bicelles at 3.9Å resolution in

an apo nucleotide-free state (Lee et al., 2016). Each subunit contains a transmembrane membrane domain that is composed of 6 α-helices, and two NBDs remain in close contact, freeing the ATP-binding site open to accept ATP molecules. The two nucleotide-binding sites (NBS) in ABCG5/G8 are catalytically asymmetric (Figure 1.3). The active and conserved site consists of the Walker A and Walker B motifs from ABCG5 and the signature motif of ABCG8. The other NBS, formed by Walker A and Walker B motifs of ABCG8 and the signature motif of ABCG5, is degenerated and inactive. The degenerated site contains two non-conserved residues on Walker A of ABCG5 (GSSGCGRAS, RA instead of consensus sequence KT), where the lysine is known to be critical for ATP hydrolysis (Zhang et al., 2006). Therefore, it has been hypothesized that ABCG5/G8 binds two ATP molecules, with only one hydrolyzed (Wang et al., 2011). The first high-resolution structure of ABCG5/G8 provided a breakthrough in revealing a more relevant molecular platform for further mechanistic studies of this transporter (Lee et al., 2016).

The atomic model has revealed several structural motifs that may play important roles in our understanding of how ABCG5/G8 or other ABC sterol transporters function (Figure 1.4) (Lee et al., 2016). First, the triple helical bundle, which consists of a coupling helix (CpH), connecting helix (CnH), and an E-helix and a Q-loop of ABC proteins is located between the NBD and TMD and may play the role of transmitting the allosteric communication between the NBD and the

TMD (Figure 1.4 A/B). Secondly, the structure of ABCG5/G8 revealed a cluster of polar amino acids in the TMD and on the triple helical bundle (Figure 1.4 C/D). These residues are well positioned within several hydrogen bonds and salt bridges, and thus might be playing an important role in stabilizing the different conformations of the transporter. Thirdly, a putative binding site of sterols was proposed to be situated in an area with close proximity to several aromatic and hydrophobic amino acids (Figure 1.4E). Site-directed mutagenesis of an alanine residue (ABCG5-A540F) in the middle of this area abolished the biliary cholesterol secretion in a transgenic mouse model, suggesting that A540 may play an important role in the translocation of cholesterol in the TMD. In addition to that, a coevolution analysis on ABCG5 and ABCG8 TMD sequences highlighted potential interactions between conserved residues that are separated by a distance of more than 8Å apart in the published structure (PDB accession number: 5DO7). These residues may come in contact at another stage, suggesting that the TMDs of ABCG5 and ABCG8 may migrate towards each other at some point in the transport cycle. The initial molecular dynamics (MD) simulations suggested that an inward and upward movement of the TMD, while the NBD showed an inward movement during the transporter cycle (Lee et al., 2016; Zein et al., 2019).

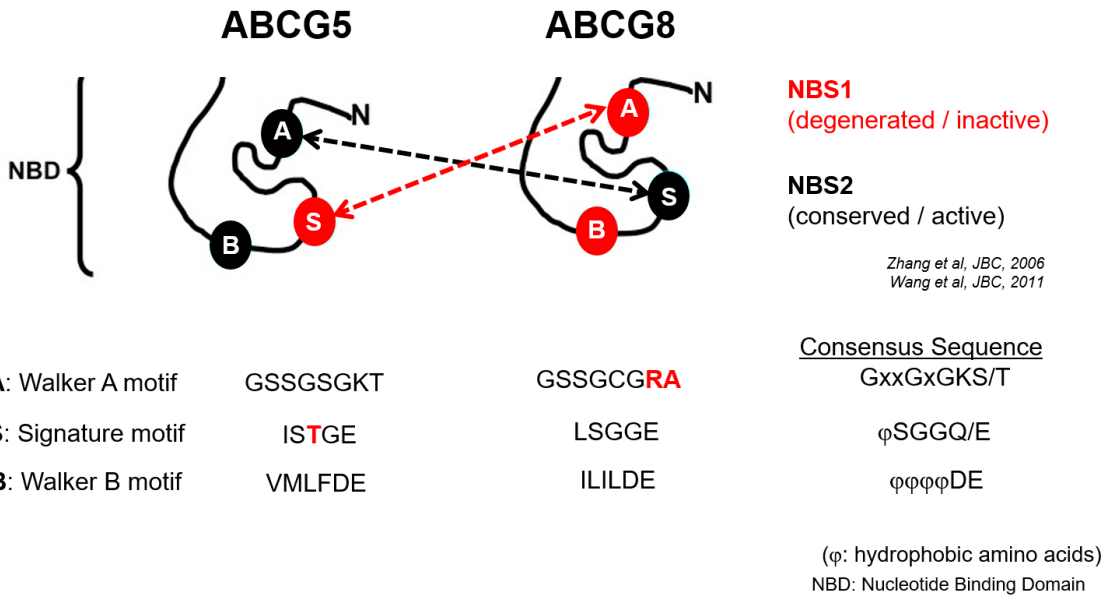

Figure 1. 3: Schematic diagram of the two nucleotide binding sites in ABCG5/G8.

Walker A, Walker B motifs on ABCG8 and signature motif on ABCG5 (Red circle) form the inactive sites. Walker A, Walker B motifs on ABCG5 and signature motif on ABCG8 (black circle) form the active sites.

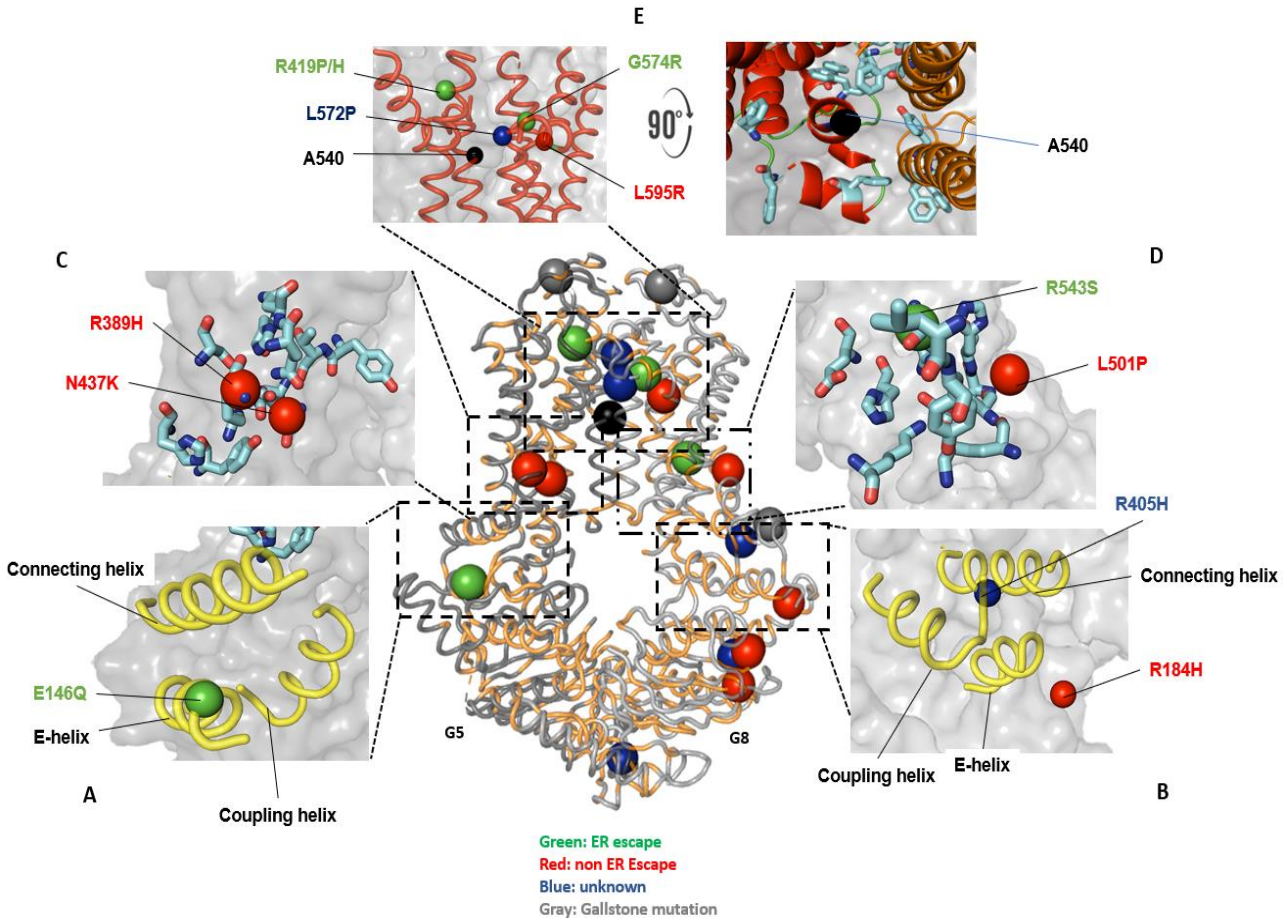

Figure 1. 4: Location of missense mutations and structural motifs of ABCG5G8. (center) Cartoon presentation of ABCG5G8 atomic model (PBD: 5DO7) with conserved amino acid colored light orange. **Spheres**: Represent the location of sitosterolemia missense mutation with different colors based on their maturation (key above). **E:** The ECD and the putative binding/entry site where a black sphere shows the A540 Residue surrounded by several aromatic residues, the effect of the mutation of this residue (A540F) along with two ER escape mutants (G5-E146Q, G8-R543S) on the ATPase activity of ABCG5/G8 was studied in my project. The two triple helical bundles, which may play a communicating role between the NBD and the TMD are shown in **A** and **B**. **C** and **D**: Stick representation of the polar amino acids in the polar relay motif which may play a very important role in stabilizing the different conformation changes of ABCG5/G8 transporter. This figure was originally published in (Zein et al. 2019)

1.7 Working Model of ABCG5/G8 Mechanism

Based on the structural interpretation of ABCG5/G8 and previous functional studies in mice and cell models (Graf et al., 2003, Graf et al., 2004, Hirata et al., 2009, Lee et al., 2016, Yu et al., 2004), my thesis research is based on a working model that describes ABCG5/G8-mediated sterol transport in cell membranes (Figure 1.5). In this model, cholesterol or other sterol molecules move to the sterol-binding site near the TMD-ECD vestibule. Recruitment of ATP molecules to the nucleotide-binding sites results in closure of the NBD dimer, and such power stroke would move the two triple-helical bundles closer. Consequently, a possible rotational movement in the transmembrane helices would drive conformational change of TMD to allow cholesterol release to the bile micelles.

In order to further define the mechanism of ABCG5/G8-mediated sterol transport, additional information is required. For example, how is ATPase activity coupled to the predicted movements during the transport cycle? As predicted by MD or co-evolution analysis, how would we know whether the projected movements in the TMD and the NBD occur at the same time or at different stages? One way to address these questions is to study missense loss-of-function disease mutations that were mapped to locations near or at the different observed structural motifs (Figure 1.4), or by further structural study of the transporter at different confirmations, which in turn would reveal the characteristics of the transporter during different transport stages.

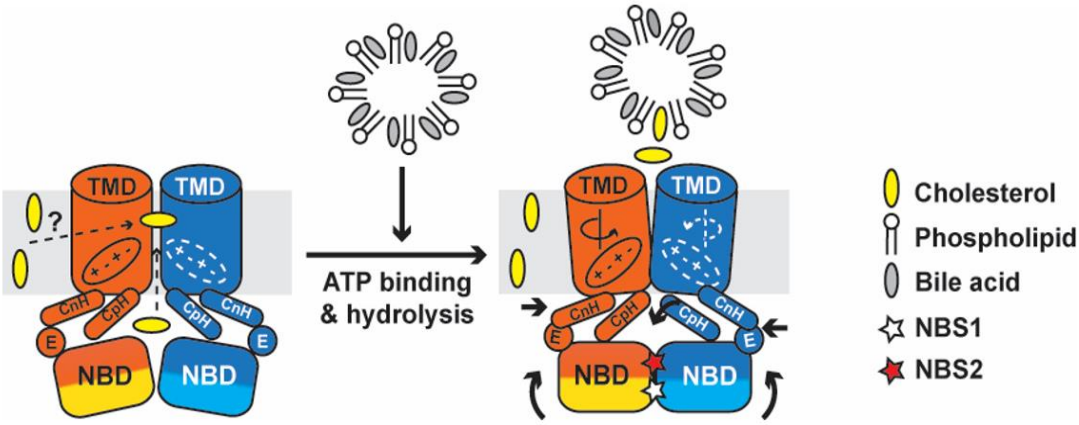

Figure 1. 5: Working model of ABCG5/G8-mediated sterol transport.

Sterol molecules move to its binding site near the TMD-ECD vestibule. Recruitment of two ATP molecules to the nucleotide-binding sites (NBS1,2), results in closure of the NBD dimer, which may bring the two triple-helical bundles (coupling helix (**CpH**), connecting helix (**CnH**), and E-helix (**E**)) closer. Consequently, a conformational change of TMD, which will be driven by a possible rotational movement in the transmembrane helices, will allow cholesterol release to the bile micelles.

1.8 Expression and Purification of Membrane Proteins

As endogenous expression is relatively low and not enough for robust *in vitro* functional and structural studies, different eukaryotic and prokaryotic systems have been used for expressing high quantity of recombinant membrane proteins (Müller et al., 2006). Common expression hosts include bacterial, yeast, mammalian, and insect expression systems for recombinant proteins (Geisse et al., 1996).

Yeast and bacterial systems are the most commonly used since in such systems it is easy to manage cell growth and they can be used to produce large quantities of protein at low cost (Nielsen et al., 2014). *E. coli*, a bacterial host, is used for large-scale production of many soluble proteins. However, due to its lack of the cell machinery for several eukaryotic post-translational modification, *E. coli* has been shown not to be ideal to manage the complexity of eukaryotic membrane proteins and often produces proteins that are incorrectly folded and modified (Karste et al., 2017). Expression of human membrane proteins is relatively complex, as it requires many post-translational modifications such as glycosylation, phosphorylation, etc. (Karste et al., 2017). Hence, yeast, mammalian or insect expression systems are the best systems for expression of such proteins (Vieira Gomes et al., 2018). Yeast, the simplest eukaryotic expression system, shares many similarities to the mammalian systems in term of post-translation modifications with significantly lower cost and higher productivity,

and has been a very good system to produce large amounts of functional human membrane proteins. For instance, the yeast system was used as a very effective system to express many ABC transporters, which were then purified into functional forms (Lee et al., 2016; Bertheleme et al., 2015).

While working with the right system is the initial and critical step, other parameters must be taken in consideration to obtain the highest yield with properly mature and functional proteins (Fernández et al., 2016). The duration of protein expression in host cells must be optimized for maximal expression, and the temperature at which cells express a certain protein can make key in obtaining a well folded and functional protein. Besides, some membrane proteins could be toxic to certain host cells and could cause cell death (Gómez et al., 2016). High integration of DNA plasmids into their expression host can cause an overexpression of the protein, a potential physiological burden to the cellular machinery, and often leads to misfolded proteins (Gómez et al., 2016). All these challenges must be taken into consideration while one is optimizing any system for protein expression. More recently, fusion proteins, such green fluorescence protein (GFP), have emerged as a good tool to overcome these challenges and result in more efficient protein maturation. The fusion-protein strategy also provides an endogenous reporter to monitor protein expression and maturation of membrane proteins (Snapp et al., 2005).

1.9 *Pichia pastoris* Yeast as a Recombinant Protein Expression System

As described above, the ability of yeast system to undergo many post-translational modifications that are critical for the proper folding and maturation of eukaryotic membrane proteins (Nielsen et al., 2014). For instance, the N-glycosylation of both ABCG5 and ABCG8 is essential for synthesis of mature heterodimers (Graf et al., 2004). In addition, it is cost-effective as yeast can easily and quickly grow in a regular molecular biology lab setting and requires minimal and simple genetic manipulation. *Saccharomyces cerevisiae and Pichia pastoris* are the most commonly used species in yeast. *Pichia pastoris is a* methylotrophic yeast, a species that can metabolize methanol as the sole carbon source (Werten et al., 2019). In our laboratory, we have developed protocols on the use of the *P. pastoris* yeast as the primary expression host for large-scale production of membrane proteins.

The methanotrophic yeast contains a very powerful methanol-regulated alcohol oxidase promoter (P_{AOX1}) and can undergo efficient post-translational modifications in eukaryotes (Krainer et al., 2012). In the shaker-growth condition, a large mass of cells (usually 20-40 grams per liter) can be obtained by growing the transformed yeast clones in a minimal glycerol yeast nitrogen base (MGY) media. To express the proteins of interest, cDNA is cloned into a bacteria-yeast shuttle vector (e.g., pPICZ) (Abdemami et al., 2011) and transformed into the yeast genome in order to create stable cell lines that constantly express the foreign

protein. The gene of interest is normally flanked by promotor sequences of AOX1, and the foreign genes are integrated into the yeast genome by homologous recombination. Clones that carry recombinant proteins are selected by antibiotic resistance to Zeocin (Krainer et al., 2012).

1.10 Membrane Protein Solubilization, Purification, and Reconstitution

Due to its hydrophobic surface, its flexibility and generally lack of stability, the expressed recombinant membrane protein remains one of most challenging reagents to work with (Patrick et al., 2003; Pandey et al., 2016). Major challenges can include: solubilization, purification and functional reconstitution. An optimal solubilization strategy is critical in large-scale extraction of pure proteins and in maintaining their active forms. In addition, the solubilization process requires disrupting the lipid components of the membrane and placing the membrane proteins in a nonnative detergent environment, which could destabilize and misfold the proteins (Patrick et al., 2003). It is thus necessary to screen a series of solubilization conditions and develop the most optimal protein-extraction protocol for functional and structural studies (Patrick et al., 2003).

Detergents are amphipathic molecules with hydrophilic groups (heads) and aliphatic hydrocarbon groups (Chaptal et al., 2017). Depending on their headgroup, detergents are generally classified into three classes: Ionic, non-ionic

and zwitterionic. Ionic detergents are usually the most effective detergents to solubilize a membrane protein but are very harsh as proteins can be destabilized and denatured (Chaptal et al., 2017). Both non-ionic and zwitterionic detergents are milder detergents and widely used in solubilization due to their ability of maintaining the integrity of the recombinant protein. Detergents with same hydrophilic heads but different aliphatic chain length may also be used in different stages of solubilization, these differential aliphatic chain lengths can be critical in downstream studies. For example, membrane protein crystal growth is often supported by shorter carbon chains while slighter longer chains are more effective in solubilization (Lee et al., 2016). The aliphatic chains of the most commonly used nonionic detergents in membrane protein solubilization vary between 10 to 14 carbons. The most commonly used detergent, n-dodecyl-β-D-maltopyranoside (DDM), consists of maltose headgroup attached to a 12-carbon aliphatic chain. Moreover, determining the concentration of the detergent is very important during the solubilization process as a minimal concentration of detergent is necessary for the formation of the required micellar structure for protein extraction, a concentration normally referred as the critical micelles concentration (CMC) (Ruckenstein et al., 1975). The aliphatic chain length affects the CMC; for example, longer chains need less molecules for the micelles to be formed, thus a lower CMC (Ruckenstein et al., 1975). In practice, during solubilization, detergents are usually used at 10 folds the CMC for membrane protein solubilization, despite the risk of

destabilizing the recombinant protein. As such, excess detergent should be removed as quickly as possible prior to subsequent purification procedures and maintained at just higher than its CMC to avoid protein denaturation and aggregation (Wolfe et al., 2017).

In addition to detergents, a new approach has been developed for membrane protein isolation and is detergent-free and avoids detergent-driven protein damage. This new method exploits styrene maleic acid (SMA) copolymers to wrap around the protein in a lipid-bilayer mimetic complex, SMA lipid particles (SMALPs) (Dörr et al., 2016). This will serve as an alternative method in our membrane protein studies.

In terms of purification, many different protocols of purifications have been reported over the years to purify a variety of membrane proteins. Usually, a protocol combines a mix of column chromatography, including gel-filtration, affinity, and ion exchange (Berg et al., 2002). Affinity chromatography takes advantage of the fusion polypeptides on the proteins of interest and specially isolate the proteins from the cell lysates. Commonly used tags include: HIS tag, CBP tag, FLAG tag, and STREP tag, and this method is by far the most successfully applied method for the initial purification of a membrane protein (Berg et al., 2002). Affinity chromatography is also used to obtain concentrated samples in a very small volume for gel-filtration or ion exchange chromatography (Berg et al., 2002).

Lipids are commonly used to activate membrane proteins (Wang et al., 2015). Purification of a membrane protein is usually followed by reconstitution into a lipid-based environment for functional studies. Reconstitution includes various formats, such as micelles, bicelles, liposomes, or nanodiscs (Frey et al., 2017), and the lipid composition in the membranes can have profound effects on the interaction of a protein with their substrates and/or can alter their functions, especially when tested in *in vitro* assays. In this thesis, I have focused on micelle-based reconstitution to execute proposed functional studies.

1.11 Objectives of the Thesis

In this thesis, to facilitate functional and structural studies, I first focused on cloning and expression of a series of catalytically deficient and disease-causing missense mutants of ABCG5/G8, as well as N-terminally truncated mutants of this heterodimer (Chapter 3). I then focused on three missense mutants to characterize their impact on the ATPase activity (Chapter 4). The central hypothesis of my research is that the disease-causing and sterol-binding mutations of ABCG5/G8 are catalytically impaired. To address this, I have carried out the following two specific aims to achieve this project.

1.11.1 Expression and purification of ABCG5/G8 WT and three missense mutants. Two of these mutants, ABCG5-E146Q and ABCG8-R453S (Figure 6), are disease-causing loss-of-function mutations located on the triple helical bundle and in the polar relay motif respectively. The other mutation, ABCG5-A540F, is located at the putative sterol binding/entry site.

1.11.2 Determine the impact of these mutants on the ATPase activity of ABCG5/G8. We have developed a high-throughput and colorimetric assay to detect ATP hydrolysis by recombinant ABCG5/G8. In the presence of the more water-soluble cholesterol analog, cholesteryl hemisuccinate (CHS,) ATP hydrolysis of the WT ABCG5/G8 displayed a maximal specific activity of an

average of ~600 nmol/mg/min which is 5-fold higher than the published results (Johnson et al., 2010). This CHS stimulated assay will be used to determine enzymatic characteristics of the ABCG5/G8 WT and the mutant proteins.

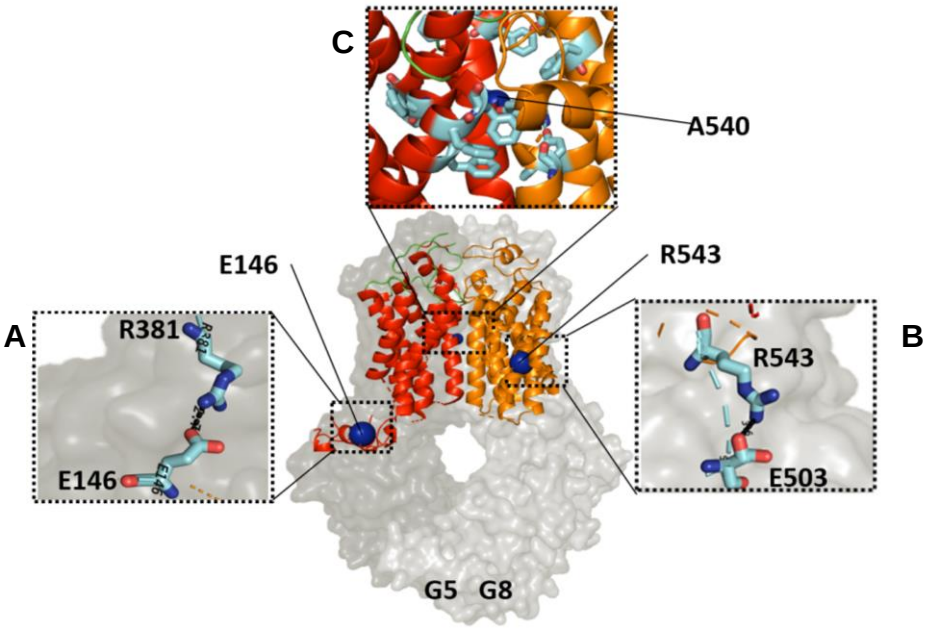

Figure 1. 6: Cartoon presentation of ABCG5G8 atomic model (PBD: 5DO7). A and B: stick representation shows the interaction between disease mutation residues with their microenvironment. **C** The putative binding/entry site where a A540 Residue surrounded by several aromatic residues.

Chapter 2: Materials and Methods

2.1 Materials

2.1.1 Cell strains, cDNA, expression vectors, and chemical reagents:

Escherichia coli XL1-Blue competent cells were obtained from *Novagen.* The *Pichia pastoris* yeast strain; KM71H, was obtained from Invitrogen. ABCG5 and ABCG8 *P. pastoris* expression vectors (pSGP18 and pLIC) were derived from pPICZB (Invitrogen) as described previously (Johnson et al., 2010). The cDNAs for human ABCG5 (NCBI accession number: NM_022436) and ABCG8 (NCBI accession number: NM_022437) were obtained from the National Institutes of Health collection (M. Dean). WT ABCG5 with a C terminal tag s was expressed with a tag of twelve histidines separated by a glycine (His_6-Gly-His_6) on its (pLIC-G5-H12) along with WT ABCG8 either with a rhinovirus 3C protease site followed by a calmodulin binding peptide (CBP) tag on the C terminus of ABCG8 (pSGP18-G8-3C-CBP) or without any tags (pSGP18-G8).

Escherichia coli polar lipids were obtained from Avanti Polar Lipids Inc. n-Dodecyl β-D-maltopyranoside (DDM), cholesteryl hemisuccinate (CHS), and cholesterol were obtained from Anatrace. Ni-NTA agarose resin was from Qiagen, and calmodulin affinity resin was from Agilent. ATP disodium trihydrate, Tris (2-carboxylethyl) phosphine (TCEP), sodium chloride, Glycerol, EDTA, EGTA, Sodium dodecyl sulfate (SDS), ponceau solution, sodium azide, Bradford

reagents, tween 20, Methanol and ammonium hydroxide, Hydrochloric acid, acetic acid, magnesium chloride, calcium chloride, and all protease inhibitors were obtained from Bioshop Canada. Biotin, Sodium cholate hydrate, L-ascorbic Acid, ammonium molybdate, bismuth citrate, and sodium citrate were obtained from Sigma Aldrich. Imidazole, ε-aminocaproic acid, sucrose, yeast extract, tryptone, peptone, yeast nitrogen base (YNB) and ammonium sulfate were obtained from Wisent INC. Dithiothreitol (DTT), Tris base, and Tris acetate were obtained from fisher bioreagents. Clarity western ECL substrate, 30 % acrylamide, Agarose and Ammonium persulfates were obtained from BIO-RAD. Restriction enzymes were obtained from new England Biolabs or Thermo-Fisher Scientific. Antibiotics Zeocin and ampicillin was obtained from Invitrogen.

2.1.2 Cell culture media (The solutions are stored in a sterile environment)

a. Stock solutions

- **10X YNB**: 100g of ammonium sulfate with 34g of yeast nitrogen base (YNB) was dissolved in 1L deionized H_2O, filtered and stored in dark sterile place.
- **1000X B**: 40mg of biotin was dissolved in 100mL deionized H_2O, filtered and stored at room temperature.
- **10X D**: 200g of D-glucose (also known as dextrose) was dissolved in 1L of deionized H_2O, autoclaved for 25 minutes on liquid cycle and stored at room temperature.

- **10X GY**: 100mL glycerol was dissolved in 900mL of deionized H_2O, autoclaved for 25 minutes on liquid cycle and stored at room temperature.

b. *E. coli* growth media:

- **Low salt LB (Luria-Bertani):** 10g of tryptone, 5g of yeast extract and 5g of NaCl were dissolved in 1L of deionized H_2O. The pH was adjusted to 7.5 with 1M NaOH before It was autoclaved and stored at room temperature in sterile environment.
- **LB agar Zeocin plates**: 15 g was added to 1-liter LB media before autoclave. The autoclaved media was cooled down to 55°C and 40ul of Zeocin (1mg/mL stock) was added, poured in petri plates and then stored at 4 °C.

c. Yeast growth media:

- **Minimal Dextrose (MD) plates**: 15 g of agar was dissolved in 800 mL deionized H_2O and autoclaved for 25min on liquid cycle, then 100mL of 10X YNB, 1mL of 1000X B, and 100 mL of 10X D were added before pour into petri plates and stored at 4 °C.
- **YPDS plates (Yeast Extract Peptone Dextrose plates)**: 10g yeast extract, 182.2g sorbitol (1M), 20g of peptone, and 20g of agar were dissolved in 900mL deionized H_2O, autoclaved for 25 minutes on liquid cycle, then 100mL 10XD was added before pour it into petri plates and stored at 4 °C. Antibiotic zeocin (100mg/mL) was added to the media before pouring into the petri plates at

different concentration; high zeocin plates 1mL per 100mL media, medium zeocin plates 0.5mL per 100mL media).

- **MGY (Minimal Glycerol Yeast nitrogen base) Medium**: 800mL of autoclaved deionized H_2O were combined with 100mL of 10XYNB, 100mL 10X GY and 1mL of 1000X B.
- **MY (Minimal yeast nitrogen base) Medium**: 900mL of autoclaved deionized H_2O were combined with 100mL of 10XYNB and 1mL of 1000X B.

2.1.3 Cell lysate and protein purification Buffers

a. **Protease inhibitors stock solution:** The protease inhibitors and their concentration used is shown below.

    - Leupeptin 10mg/mL in water
    - Pepstatin A 10mg/mL in dry DMSO
    - Chymostatin 2.5 mg/mL in dry DMSO
    - PMSF 1M in dry DMSO

20 ul of leupeptin, pepstatin, and chymostatin and 100 µL of PMSF were only added to every 100mL buffer immediately prior to use. All the protease inhibitors were obtained from Bioshop.

b. **mPIB Yeast cell lysis buffer:** 0.33 M sucrose, 0.3 M tris-HCl (pH 7.5), 1 mM EDTA, 1mM EGTA, 100mM ε-aminocaproic acid, add H_2O to a final volume 1 L and stored at 4 °C.

c. **Buffer A, Microsomal membranes buffer:** 50mM Tris pH 8, 100mM NaCl, 10% glycerol.

d. **Membrane protein solubilization buffer:** 50mM Tris pH 8, 100mM NaCl, 10% glycerol, 2%DDM, 1% Na cholate, 0.2% CHS, 10mM β Mercaptoethanol.
e. **Buffer B, Ni-NTA wash buffer:** 50 mM Tris pH 8, 100 mM NaCl, 0.1% β-DDM, 0.05% cholate, 0.01% CHS, 1 mM TCEP.
f. **Buffer C, Calmodulin wash buffer:** 50 mM Tris pH 8, 100 mM NaCl, 0.1% β-DDM, 0.05% cholate, 0.01% CHS, 1 mM TCEP, 1 mM $CaCl_2$ and 1 mM $MgCl_2$.
g. **Buffer D, CBP elution buffer:** 50 mM tris, pH 8, 300 mM NaCl, 2 mM EGTA, 0.1% DMM, 0.05% cholate, 0.01% CHS, 1 mM TCEP.
h. **Buffer E, Ion exchange Diethylaminoethyl (DEAE) buffer:** 20mM tris-acetate pH 6, 0.1% DDM
i. **Buffer G, Size exclusion chromatography (SEC) buffer**: 50 mM Tris pH 8, 100 mM NaCl, 0.1% DMM, 0.05% cholate, 0.01% CHS, 1 mM TCEP (filtered at 0.2µ).
j. **Tris-Buffered Saline, 0.1% Tween (TBST):** 20 mM Tris-HCl pH 7.5, 1M NaCl; 0.2% Triton X-100, 0.05% Tween 20
k. **Western blot transfer buffer:** 194 mM glycine, 15 mM Tris base, 20% methanol

2.1.4 ATPase assay buffers

a. **Protein** (Fig. 3.12): WT ABCG5/G8 of 0.7 µg/µL, ABCG5-A540F/G8 of 0.4 µg/µL, ABCG5-E146Q/G8 of 0.5µg/µL, ABCG5/G8-R543S of 0.4µg/µL, and ABCG5/G8- G216D of 0.6µg/µL all protein were stored at -80°C upon

purification in **ATPase buffer:** 50mM Tris pH 7.5, 100mM NaCl, 0.1% DDM, 0.05% cholate, 0.01% CHS.

b. **Cholesteryl hemisuccinate (CHS):** 0.5% CHS stock solution in 3% Na Cholate, 50mM Tris pH 7.5, 100mM NaCl. The stock was stored at -20°C
c. **10X ATP cocktail:** 50mM ATP, 75mM MgCl2, 100mM NaN3, 50mM Tris Cl 7.5. Cocktail was stored at -20°C
d. **Quenching solution:** 5% SDS and 5mM HCl in Filtered H_2O was stored at room temperature.
e. **Potassium phosphate standards:** 0nM, 0.125nM, 0.25nM, 0.5nM, 1nM, 2nM inorganic phosphate concentrations in 50mM tris-Cl pH 7.5 were stored in the dark at room temperature.
f. **Methyl-β-cyclodextrin-cholesterol conjugate:** 0.5mM cholesterol in 5mM MβCD, 1mM cholesterol in 10mM MβCD, and 10mM cholesterol in 100mM MβCD were prepared and stored at room temperature.
g. **Methyl-β-cyclodextrin-stigmasterol conjugate:**

   0.5mM stigmasterol in 5mM MβCD and 1mM stigmasterol in 10mM MβCD were prepared and stored at room temperature.

2.1.5 Primers

The forward and reverse primers list in the table below were ordered and synthesized from Eurofins Genomics Canada.

Molecular cloning	Primers
G5-A540F	Forward: CCATTTTTGGGGTGCTTGTTGGATCTGGATTCCTCAG Reverse: GCACCCCAAAAATGGACAGCAGAGCCACTACAC
G5-E146Q	Forward: GCGCCAAACGCTGCACTACACCGCGCTGC Reverse: CAGCGTTTGGCGCACGGTGAGGCTGCTCAG
G5-R419H	Forward: GGACCATGTAGGTCTCCTTTACCAGTTTGTGGGCG Reverse: GAGACCTACATGGTCCTGGATAGCACCCTTTAGC
G5-R419P	Forward: CAGGACCCAGTAGGTCTCCTTTACCAGTTTGTGGGC Reverse: GACCTACTGGGTCCTGGATAGCACCCTTTAGCACATTG
G8-G574E	Forward: GCCGAAGGCTTCATGATAAACTTGAGCAGCCTGTGG Reverse: CATGAAGCCTTCGGCGAGGTAGAAGGAGTTGTAGAGG
G8-G574R	Forward: GCCAGAGGCTTCATGATAAACTTGAGCAGCCTGTGG Reverse: CATGAAGCCTCTGGCGAGGTAGAAGGAGTTGTAGAGG
G8-R543S	Forward: GTTGCTCTATTATGGCCCTGGCCGCCGC Reverse: GCCATAATAGAGCAACAGAAGACCACCAGCCAC
G5-dN30	Forward: GAATGCTCGAGCCTCACAGCCTGGGCATC Reverse: GAGGCTCGAGCATTCTTTTACCTCGTTCG
G8-dN15	Forward: GAATGCTCGAGGATACCTCGGGCCTCCAG Reverse: GTATCCTCGAGCATTCTTTTACCTCGTTC
G8-dN20	Forward: GAATGCTCGAGGATAGATTGTTCTCCTCTG Reverse: CTATCCTCGAGCATTCTTTTACCTCGTTC
G5-E218Q	Forward: GTTTGATCAACCAACCACAGGCCTGGACTGCAT Reverse: GGTTGGTTGATCAAACAGCATGACCTTAGGATCCTG
G5-H250S	Forward: GTTCTCACCATTTCTCAGCCCCGTTCTGAGCT Reverse: TGAGAAATGGTGAGAACCACAATTCGGTTCCTGCG
G5-K92M	Forward: ATGACCACGCTGCTGGACGCCATGTCCGGG Reverse: CAGCAGCGTGGTCATCCCGGAGCCTGAGCTTC
G8-E238Q	Forward: CAACCCACCTCTGGGCTCGACAGCTTCACAGCCC Reverse: CCCAGAGGTGGGTTGGTCGAGAATAAGGATTCCTGGG
G5-G196D	Forward: CATTTCCACGGACGAGCGGCGCCGGG Reverse: TCGTCCGTGGAAATGCCCCCCAAGCTGTAGTTGC
G8-G216D	Forward: ACGAGCGCAGGAGAGTCAGCATTGGGGTGCAG Reverse: CTCTCCTGCGCTCGTCCCCCGACAACCCC
G8-H270S	Forward: TCTCAGCCTCGCTCTGACATCTTCAGGCTGTTTGATC Reverse: AGAGCGAGGCTGAGAGAGGGAGATGAGCACCAGC
G8-R111M	Forward: TGGCCTCCTTGCTAGATGTGATCACTGGCCGAG Reverse: CTAGCAAGGAGGCCATCCCACAACCTGAGCTCC

2.2 Methods

2.2.1 Molecular cloning

a. PCR reaction

The primers for twelve-point mutations and three N terminal deletions (section 2.1.4) were designed in a way that the melting temperature of the overlapping bases of the forward and reverse primers is lower than the melting point of the neighboring base pairs to avoid any primers dimerization during the reactions. DMSO was added to the reactions to enhance the PCR amplification as it forms hydrogen bonds which DNA template which destabilize the double helix, especially for high GC rich samples (Chakrabarti et al., 2001). The primers of G5-dN30, G8-dN15, and G8-dN20 were also used to introduce a Xho1 restriction site to facilitate confirmation of the deletion. The primers were diluted to a concentration of 4μM from the stock 100μM prior to setting up the reactions. **pLIC-ABCG5-RGSH6-G-H6** and **pSGP18-ABCG8-3C-CBP** were used as WT template to either ABCG5 or ABCG8 mutations.

A 50µl PCR reaction was carried out using Phusion High-Fidelity DNA Polymerase (New England Biolabs) was set up as follows:

- 10µl Phusion buffer
- 1µl dNTP
- 26.5µl H_2O
- 1µl DMSO
- 1µl DNA template (100ng/µl) (pLIC-ABCG5-RGSH6-G-H6 / pSGP18-ABCG8-3C-CBP)
- 5µl Forward primer (4µM)
- 5µl Reverse primer (4µM)
- 0.5µl DNA Polymerase

The PCR settings were as follows:

STEP	TEMP	TIME	NUMBER OF CYCLES
INITIAL DENATURATION	**98°C**	**2 min**	
DENATURATION	**98°C**	**15 sec**	
PRIMER ANNEALING	**55°C**	**30 sec**	**30**
EXTENSION	**72°C**	**3 min**	
FINAL EXTENSION	**72°C**	**20 min**	
HOLD	**4°C**	**∞**	

b. Confirmation and DNA cleaning

The confirmation of the amplification of was verified by running 5µl of the PCR products on 1% agarose gel in TAE buffer. After confirmation, 1µl of Dpn1 restriction enzyme was added to each sample and incubated overnight at 37°C to digest the WT plasmid templates. The modified plasmids were cleaned up by ethanol acetate precipitation:

5µl of 3M Sodium acetate was added to 50µl PCR product. 200µl of 100% Ethanol was added to each tube, vortexed, and left at room temperature for 10 minutes. The DNA was precipitated by centrifugation at maximum speed in an Eppendorf centrifuge for 10 minutes. The supernatant was discarded, and the DNA pellet was washed with 75% ethanol. Following high speed centrifugation, residual ethanol was discarded and completely evaporated by vacuum centrifugation for 20 minutes. The pellet was then resuspended with 10µl deionized H_2O.

c. Transformation into XL1 blue *E. Coli* competent cells (heat shock)

50µL of competent E. coli cells was placed in each of the 1.5 mL Eppendorf tubes with 1µg of the modified plasmids and incubated on ice for 1 hour. The samples were heat shocked by incubating the tubes at 42ºC for 45 seconds, then placed back on ice for 2 minutes. 950µl of LB media was added to each tube and transferred to 5ml cultured tubes. Cultures were incubated in a 37ºC shaker for 1 hour at 250 rpm. Next, the cells were pelleted and resuspended in 100µl of LB,

then cultured onto a LB-zeocin plates which were incubated at 37ºC overnight. Three colonies were picked from each of the transformation plate of the 15 different mutations using a sterile thin pipette tip and dipped into a fresh 100mL LB-zeocin media which were left on the shaker overnight at 250 rpm and 37ºC. Then the grown cells were pelleted for DNA isolation.

d. DNA isolation and sequencing

The plasmids were purified by PureYield Plasmid Midiprep kit (Promega Canada) following the manufacture's protocol (technical manual #TM253). The isolated plasmids were sequenced at Eurofins Genomics Canada facility to confirm the presence of mutations.

2.2.2 Nomenclature of Constructs

Following DNA sequencing, 22 different constructs were created where modified or WT pSGP18-ABCG5 and WT pSGP18-ABCG8 were co-transformed into *P. pastoris* KM71H strain by electroporation according the table 2.1.

Construct		pLIC-ABCG5	pSGP18-ABCG8
1	Missense Mutation	R419H	WT
2		E146Q	WT
3		A540F	WT
4		WT	R543S
5		WT	G574R
6		WT	G574E

7		**R419P**	**WT**
8	**Catalytic mutations**	**H250S**	**H270S**
9		**E218Q**	**E238Q**
10		**H250S**	**WT**
11		**WT**	**H270S**
12		**E218Q**	**WT**
13		**WT**	**E238Q**
14		**G196D**	**WT**
15		**WT**	**G216D**
16		**K92M**	**WT**
17		**WT**	**R111M**
18	**Truncated G5G8**	**WT**	**dN15**
19		**WT**	**dN20**
20		**dN30**	**WT**
21		**dN30**	**dN15**
22		**dN30**	**dN20**

2.2.3 Transformation into *P. pastoris* yeast

a. Linearization of the plasmids by PmeI restriction enzyme: 20µg of each plasmid was added to a 1.5ml Eppendorf tube. The volume was adjusted to 88µl depending on the plasmid concentration, 10µl Cutsmart buffer and 2µl PmeI enzyme were added and incubated overnight at 37ºC. Then, DNA were cleaned following same procedure explained above (2.2.1 b).

b. Preparation of electrocompetent KM71H *P. pastoris* cells for transformation: Prior to the transformation, naïve cells were prepared as follows: 10 mL of YPD media was inoculated using a sterile loop with KM71H cells in a sterile 50 mL capped tube and grown overnight at 250 rpm and 30°C. The grown cells were then added into 100 mL of YPD media in a 250 mL flask to an OD_{600} of 0.1. The cells were grown for 8-10 hours to reach an OD_{600} of 1 at 250 rpm and 30°C. Then the cells were centrifuged at 5000×g for 10 minutes and resuspended in 200 mL of sterile deionized H_2O. The cells were centrifuged again for 10 minutes (repeated the H_2O wash twice). The pellet was resuspended in 40 mL of sterile 1M sorbitol. Then the cells were centrifuged at 5000×g for 10 minutes and resuspended in 2.4mL 1M sorbitol and were chilled on ice before transformation.

c. Electroporation: The linearized plasmids, (pSGP18-ABCG5 and pSGP18-ABCG8) according to the table in section 2.2.1 e, were combined with 80µl sorbitol-yeast cells on ice, then transferred to MicroPulser Electroporation Cuvettes (BIO-RAD Canada). The electroporation was done using MicroPulser Electroporator (Bio-Rad) with the preset program for *P. pastoris* yeast.

d. Cells recovery: After electroporation, the cells were immediately resuspended in 1mL of ice cold 1M sorbitol and incubated at 30°C for 1 hour. Then 5mL fresh YPD was added and incubated for 6 hours at 250 rpm and 30°C. the

cells were then centrifuged at 3000xg for 10 minutes and resuspended in 200µL of YPD. 100 µL of transformants were plated on YPDS plates containing 500, and 1000 µg/mL Zeocin to screen for successful transformants with multicopy integration. Plates with only naïve cells without plasmids were used as negative control.

2.2.4 Recombinant ABCG5 and ABCG8 expression:

a. Small scale: For each mutant, 7 individual colonies were picked from high zeocin plates and re-plated on YPD plates. After two days, the colonies were grown in 10 mL of MGY media for 24 hours in sterile 50 mL tubes at 250 rpm and 30°C. The cells were centrifuged for 10 minutes at 3000xg and the resuspended in 10 mL of MM media. 50 µL methanol was added to the media and once every 12 hours.

The cells were harvested after 24 hours incubation at 250 rpm and 30°C and resuspended in 600µL mPIB buffer and transferred to a 1.5 mL Eppendorf tube. Upon addition of 500 µL glass beads, protease inhibitors, and 10mM DTT, the cells were lysed in a mini-bead beater (Biospec) for 1.5 minutes and rested on ice for 1.5 minutes (3 repeats). The unbroken cells and beads were pelleted by centrifugation at 5000×g for 5 minutes at 4°C then at 21130xg for 5minutes at 4°C. The supernatant was collected, and the concentration of the total protein determined by a Bradford assay: 1 µl of cell lysate alongside a 0 µg to 10 µg BSA

standard were added to a 96 well plate. 200 µl Bradford reagent was added to each well and measurement was performed by recording the absorbance at 595 nm using a Synergy H1 Hybrid microplate reader.

b. Western blotting: Crude cell lysates were resolved on a 10% SDS- PAGE gel then transferred to a Polyvinylidene fluoride (PVDF) membrane for 75 minutes at 90V in the transfer buffer. Membranes were then incubated with Ponceau (Sigma) solution to estimate lysate concentration loaded in each lane. The membranes were then incubated in a blocking buffer (10% skimmed dry milk in TBST buffer) for 1 hour at room temperature, followed by an incubation overnight at 4ºC with polyclonal anti-ABCG8 or monoclonal anti-RGS-His4 antibody (Novus Biologicals) which were diluted 1:1000 in TBST buffer. The membranes were washed with TBST buffer three times each for 5 minutes, incubated with an anti-mouse conjugated to horseradish peroxidase (HRP) secondary antibody (diluted 1:10,000 in TBST and 3% milk) for 1 hour at room temperature. The membranes were then washed three times with TBST each for 5 minutes. Finally, membranes were incubated for 5 min with a chemiluminescence substrate, ECL (Clarity Western ECL Substrate-BIO-RAD) and protein bands were detected using a ChemiDoc XRS+ System (BIO-RAD). Mutant protein expression was quantitated using Image-J was used to quantify intensity protein band density was compared

to WT band density loaded as a positive control and the colonies with highest band density for both ABCG5 and ABCG8 were picked and stored in -80 ºC.

2.2.5 Large-scale *P. pastoris* cultures

Large scale cultures of P. pastoris expressing ABCG5/G8 variants were performed according to Lee et al., 2016. Transformed cells were grown on MD plates, 50 µL of cells from a glycerol stock were added to an MD agar plate and spread evenly using a sterile loop and incubated at 30 ºC for 2 days then stored at 4 ºC to be used for 1-2 months. Six tubes of 10 mL of MGY media were inoculated using a sterile loop with transformed cells in sterile 50 mL capped tubes and grown for 24-48 hours at 250 rpm and 30°C. Each tube was used to inoculate 1 L MGY medium in a 2.8 L Fernbach flask. A total of 6-liter cell culture was grown at 30ºC and 250 rpm in an Innova 43 shaker (New Brunswick), the pH was adjusted periodically with 1-4 mL of 10% ammonium hydroxide and maintained at pH 5-6. When the pH stabilizes, the culture was left to grow for 12 hours before induction of protein expression. 1 mL of 100% (0.1% v/v) methanol was followed by 5 mL of 100% methanol after 6-12h, and additional 5 mL of 100% methanol (0.5% v/v) every 12 hours for 36-48 hours. The cells were harvested at 4200 rpm for 20 minutes at 4 ºC. the pellets were then resuspended in lysis buffer (1mL buffer per 1g of cells) and stored at -80 ºC. (Approximately 40 ± 5 g of cell mass was typically obtained from 1 liter of cultured cells).

2.2.6 Identification of the optimal temperature of mutant expression.

To identify optimal expression conditions for the ABCG5/G8 mutants, the cells were grown and induced at three different temperatures (30ºC, 25ºC, and 20ºC). Protein expression was found to be optimal at 20ºC, although more experiments will need to be repeated to fine-tune the expression temperature. In this thesis, the expression of all mutant ABCG5/G8 was done following the protocol established for WT but with minor changes. Briefly, when the cells were grown for 24-48 hours, and the pH of the media was stable, the temperature was dropped to 20°C, 6-12 hours before the cells were fed by 1 mL methanol.

2.2.7 Microsomal membrane preparation

The Frozen cells were thawed and lysed using a C3-Emulsifier (Avestin) in a lysis buffer with protease inhibitors and 10 mM DTT. The cells were passed in the emulsifier three times at 25,000–30,000 psi. The samples were then centrifuged at 4,000 xg for 15 min followed by 15,000 xg for 30 min, all at 4 °C to separate the unbroken cells and organelles. The supernatants were poured into 70 mL Polycarbonate Bottles (Beckman Coulter) then spun at 42,000rpm in a Beckman 45Ti rotor for 2 hours at 4°C to pellet the microsomal membranes. Microsomes were suspended with a Dounce homogenizer in microsomal membranes buffer with protease inhibitors and stored at -80°C.

2.2.8 Protein purification

The purification of WT and mutant ABCG5/G8 was carried out following the established protocol with minor modifications (Lee et al., 2016).

a. Microsomal membrane Solubilization

Prior to detergent solubilization, the microsomes were rapidly thawed and diluted to 10 mg/mL in buffer A. An equal volume of solubilization buffer was added to the microsomes in addition to the protease inhibitors. The proteins were then placed on stirrer for 1 hour at 4 °C, followed by 20 minutes at room temperature. The microsomes were then centrifuged at 30000 rpm in a Beckman 45Ti rotor for 30 minutes at 4 °C. The supernatant was then kept on ice for protein purification.

b. Tandem Affinity Chromatography:

The soluble membrane proteins were either passed through a nickel-nitrilotriacetic acid (Ni-NTA (Qiagen)) column or incubated with the Ni-NTA resin for maximum 12 hours (the Ni-NTA resin was pre-equilibrated with buffer A). The column was washed with 10 column volumes with buffer B plus 25 mM imidazole and another 10 column volumes of Buffer B but with 50 mM imidazole. Proteins were eluted with Buffer B with 200 mM imidazole and collected in 1/3 column volume fractions.

Peak fractions were determined by Bradford assay, which were combined and diluted in 2-folds of Buffer C. Then the proteins were passed through calmodulin binding peptide (CBP) resins column, which was pre-equilibrated with wash buffer C. The resins were then washed with 10 column volumes of CBP resin wash buffer C. Proteins were then eluted with buffer D and collected in 1/3 column volume fractions. Peak fractions were determined through a Bradford assay. The peak fractions were then combined and concentrated to 0.5-1mL in a 100 kDa molecular weight cut-off concentrator spun at 3000g in 5-minute intervals at 4°C.

c. Diethylaminoethyl (DEAE) ion exchange chromatography:

The affinity purified proteins were dialyzed using a 100k cutoff membrane which was placed in an 1L ice chilled tris-acetate Buffer F for 3 hours (the step was repeated twice). The proteins were then passed through a 20 mL DAEA resin (pre-equilibrated with 5 column volumes of 1M tris-acetate-PH 6 followed by 5 column volumes of buffer E). The resin was washed with 2 column volumes of buffer E followed with 2 column volumes buffer E containing 50 mM NaCl. The proteins were Eluted with 2 column volumes Buffer E with 175mM NaCl and left on ice for the next step. Proteins purified with or without DEAE columns resulted in similar ATPase activity. Therefore, for functional assays in this thesis, the ion-exchange chromatography was omitted for protein preparations.

d. Size exclusion chromatography:

560 µL E. coli lipids/chloroform (14 mg) was placed inside a conical glass test tube. The it was dried under a slow stream of Nitrogen gas. The dry tubes were then placed in a vacuum pump to make sure the residual chloroform is completely evaporated, and a thin film of lipid was formed on the bottom of the tube. 1mL of ATPase buffer with 2.1% sodium cholate was added to the tube, which subjected to sonication until a clear solution. The lipid solution was then stored at -20°C.

2.2.9 ATPase activity

***a. E. coli* polar lipids (Avanti 100500C-100mg; 25 mg/mL in chloroform)**

560 µL E. coli lipids/chloroform (14 mg) was placed inside a conical glass test tube. The it was dried under a slow stream of Nitrogen gas. The dry tubes were then placed in a vacuum pump to make sure the residual chloroform is completely evaporated, and a thin film of lipid was formed on the bottom of the tube. 1mL of ATPase buffer with 2.1% sodium cholate was added to the tube, which subjected to sonication until a clear solution. The lipid solution was then stored at -20°C.

b. Detection Reagents of free inorganic phosphate

All the reagents were prepared following a published protocol (Cariani et al., 2004).

- Solution I: 10% Ammonium Molybdate, 1g Ammonium Molybdate was dissolved in 10 mL H_2O and stored at room temperature.
- Solution II: 300 mg Ascorbic acid was dissolved in 5mL H_2O. 5ml 1M HCl was added and it was cooled on ice to 4°C before addition of 0.5mL Solution-I with rapid stirring and stored on ice. Solution-II can be used up to four hours if stored on ice or can be frozen at -80°C for usage up to two months.
- Solution-III: 1.75 g Bismuth Citrate was dissolved in 50mL 1M HCl, then 1.75g Sodium Citrate was added to it. It was wrapped in aluminum foil and stored in dark place.

c. Methyl-β-cyclodextrin (**Mβ-CD**)-**Cholesterol/stigmasterol solution:**

Stock solution of 100mM Mβ-CD: 1.303 g of Mβ-CD was dissolved by vertexing in 10mL H2O.

10mM Cholesterol/Stigmasterol: 38.66 mg cholesterol or 41.26 mg stigmasterol was first dissolved in 10ml ethanol (100%).

The solution of 1 mM of cholesterol/Stigmasterol to 10mM MβCD was prepared as described. MβCD solution was heated at 80°C, and then cholesterol or stigmasterol (in ethanol) was added. The mixture was placed in 10ml glass tube, sealed and stirred in a hybridization oven at 80°C until the initially precipitated cholesterol was completely dissolved (Hirayama et al., 2013).

d. ATPase assay

- Lipid mix was prepared in ATPase buffer with:
    - 0.2% (4.11 mM) CHS
    - 1.5% Na Cholate
    - 2.1µg/µL PLE. coli
    - 2mM DTT

- 65 µL total volume reactions were prepared with:
    - 16.92µL ATPase Buffer
    - 9.28µL of PLE. coli (14mg/ml in 2.1% Cholate)
    - 1.3µL of 100mM DTT
    - 26µL 0.5% CHS in 3% Cholate
    - 6.5µL of 10X ATP cocktail
    - Protein 5µL

Prior to every experiment, 25µl of quenching solution was added to a 96-well plate and sufficiently chilled on ice. The ATPase assays were performed in 1.5 mL Eppendorf tubes in a 65 µL total volume. The lipid mix was sonicated for 10 min and then 5 µL protein was added, thoroughly vortex, and incubated at 37°C water bath for 10 min. The reactions were initiated upon addition of 6.5µl of 10X ATP cocktail. Then 8.5µl was removed at designated time intervals (0s, 2, 4, 6, 8, 10,

12 min) and quenched in the 96 well plates with quenching buffer. Inorganic phosphate with different concentration were added to the quenching solution and used as concentration standards. 50µL of Solution II was added to plate wells and left on ice for 10 min on ice. Then 75µl Solution III was added and left to incubate at 37°C for 10 minutes. The absorbance was measured at 695nm using multi-well plate reader (Synergy H1, BioTek).

Chapter 3 Results- Cloning, Expression and purification of ABCG5/G8 Mutants

3.0 Rationale:

This chapter describes the first objective of my research plan: to establish the necessary reagents for the structural and functional analysis of ABCG5/G8. In this study, *Pichia pastoris* yeast was used as the expression host to produce the mutant and WT recombinant proteins of ABCG5/G8. *Pichia pastoris* has been demonstrated to be the optimal expression host of WT human ABCG5/G8 (Lee et al., 2016). This is an inexpensive system, therefore large volumes of cells can be easily cultured allowing high-yield protein production, which is critical for structural and functional studies. Additionally, yeast possess eukaryotic protein biosynthesis machinery, especially the post-translational modifications such as glycosylation that are important for the proper maturation and localization of eukaryotic membrane proteins.

3.1 Molecular Cloning of ABCG5/G8 mutants

Site-Directed Mutagenesis was used to generate the missense disease-causing, as well as catalytically deficient, mutations (Table # 2.1, Section 2.2.2). Based on the apo crystal structure (PDB #: 5DO7), I sought to remove the predicted mobile and disordered N-termini in ABCG5 and ABCG8. Therefore,

recombinant ABCG5/G8 was engineered with N-terminal truncations of different lengths. These truncations include deletion of the N-terminal 30 amino acids in ABCG5 and deletion of the N-terminal 15 or 20 amino acids in ABCG8. (The plasmid maps with WT human ABCG5 or ABCG8 genes used in this study are shown in Figure 3.1.).

The PCR products shown in Figure 3.2 confirmed the amplification of mutant DNA constructs using agarose gel electrophoresis. After EcoRI enzyme restriction digestion, a DNA band of ~5k base pairs (bp) was resolved on the 1% TBE agarose gel (Fig. 3.2 B, C), indicating efficient amplification of the correct construct size. For the N-terminal truncation of ABCG5 or ABCG8, as explained in section 2.2.1, a XhoI site was introduced to remove designated sequences and connect the Kozak sequence to the new N-terminus. The truncated constructs were confirmed by a double restriction digestion by using EcoRI and XhoI restriction enzymes (Fig. 3.2 A). The newly engineered plasmids were then transformed into the competent *E. coli* cells for construct selection. The presence of a Zeocin resistance gene in both ABCG5 and ABCG8 expression vectors enabled a positive selection in *E. coli* transformation. Five *E. coli* colonies were picked for each modified plasmid from its corresponding plate. All the modified plasmids were then extracted by DNA mini preparation using a Promega kit, and the mutant sequences were confirmed using fee-based services at Eurofins genomics sequencing facility. Figure 3.3 shows the sequencing results for each deletion and point mutation. Following sequencing

verification of each of the mutations, the respective DNA samples were linearized and transformed into the KM71H strain of *P. pastoris* by electroporation. The transformed cells were plated onto YPDS agar plates containing various concentrations of zeocin antibiotics to ensure that only successfully transformed cells would grow on the plates, due to the presence of the zeocin gene in the integrated plasmids. To express ABCG5/G8 heterodimers, two constructs, each carries one of the two human genes ABCG5 and ABCG8, were transformed into *P. pastoris* yeast cells simultaneously. We then selected high-zeocin resistant colonies for expression analysis, as high resistance to zeocin usually results in high copy-number integration of plasmids. Ten clones were picked for each respective mutation from its corresponding high zeocin plate for additional expression tests and subsequent protein purification. ABCG5/G8 was expressed in each these colonies, and the membranes were prepared, as mentioned in section 2.2.4, resolved by SDS-PAGE and screened for ABCG5 and ABCG8 expression by immunoblotting using antibodies for anti-RGSHis4 and anti-ABCG8 antibodies, respectively. The expression of the newly transformed colonies was compared to WT expressing cells which were grown and lysed under similar conditions. Expression of both ABCG5 and ABCG8 proteins were analyzed in all the samples from the different colonies for each mutation. In Figure 3.4, the colonies, which showed the highest expression of both ABCG5 and ABCG8, were selected for further studies.

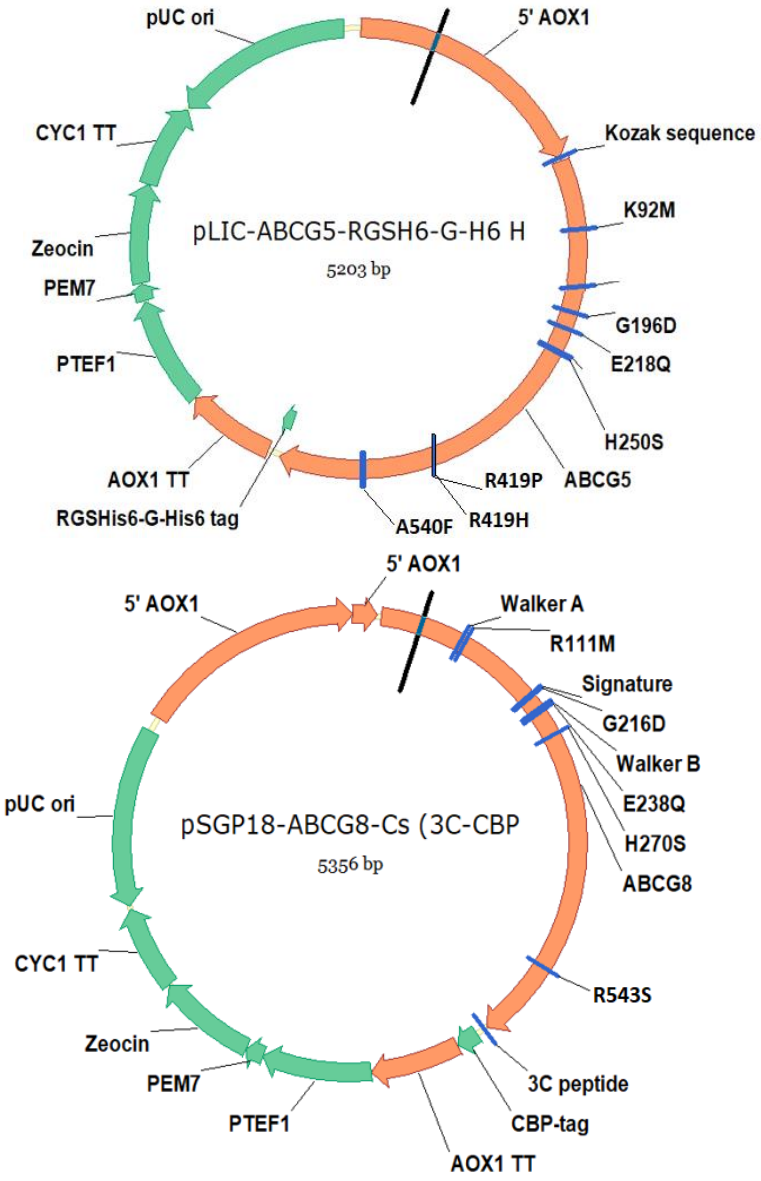

Figure 3. 1: Schematic diagrams of the ABCG5 and ABCG8 constructs.
The maps of pPICZ-derived plasmid of WT ABCG5 gene that carries a C-terminal RGSHis6-G-His6 tag (Top) and of WT ABCG8 gene carries a C-terminal CBP tag preceded by a 3C cleavage site (Bottom). Point mutations are labeled on the WT residues of each gene. The vectors have a zeocin resistance gene for positive selection of transformants in *E. coli* and *P. pastoris*. An AOX1 promoter located upstream of the foreign genes is used for protein expression. Generated by Benchling.com 2019.

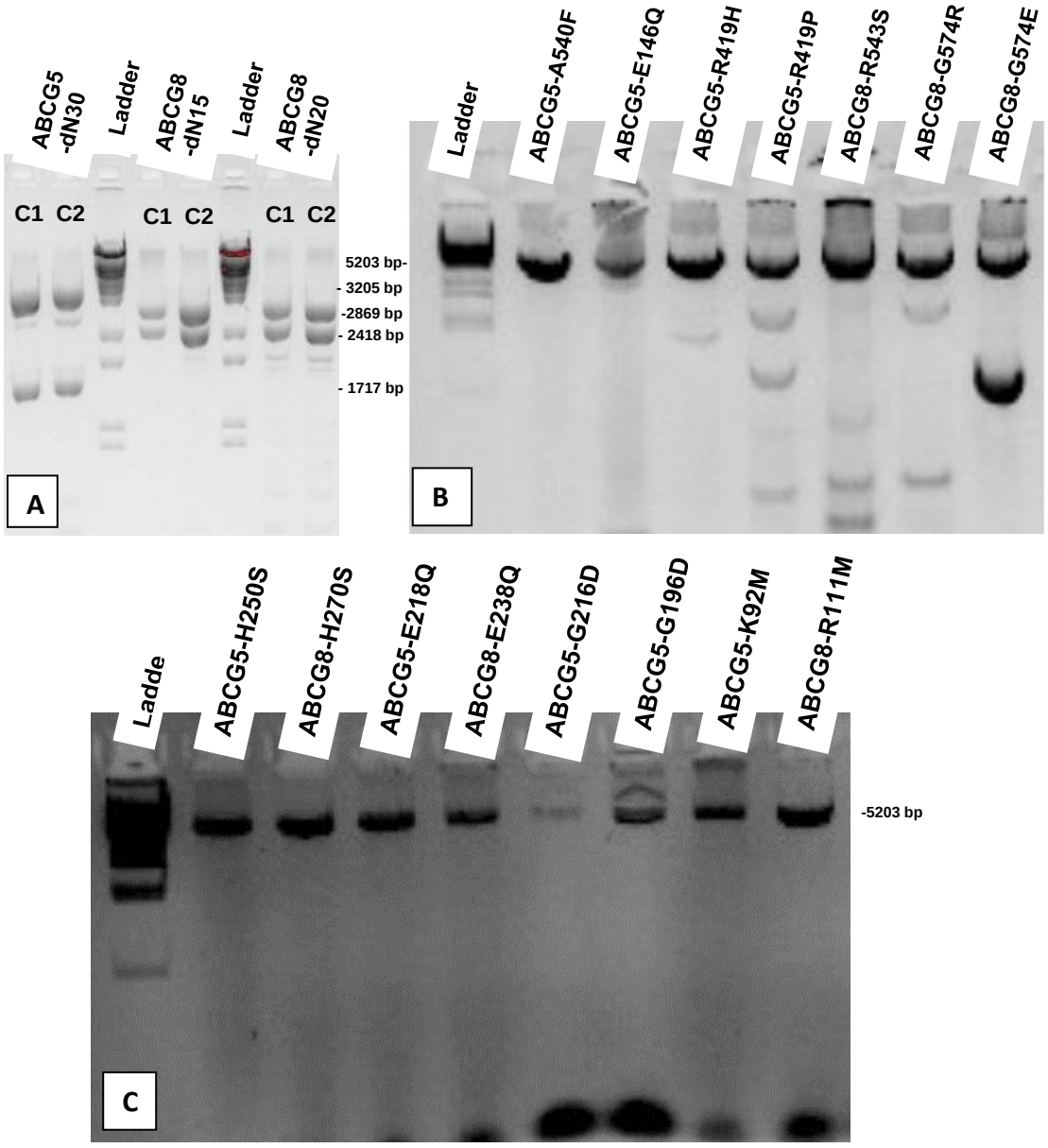

Figure 3. 3: Site Directed Mutagenesis.
The PCR products were resolved on the 1% TBE agarose gel and stained with ethidium bromide. The amplified DNA products are located at the correct molecular weight levels, confirming the effective amplification of each gene.

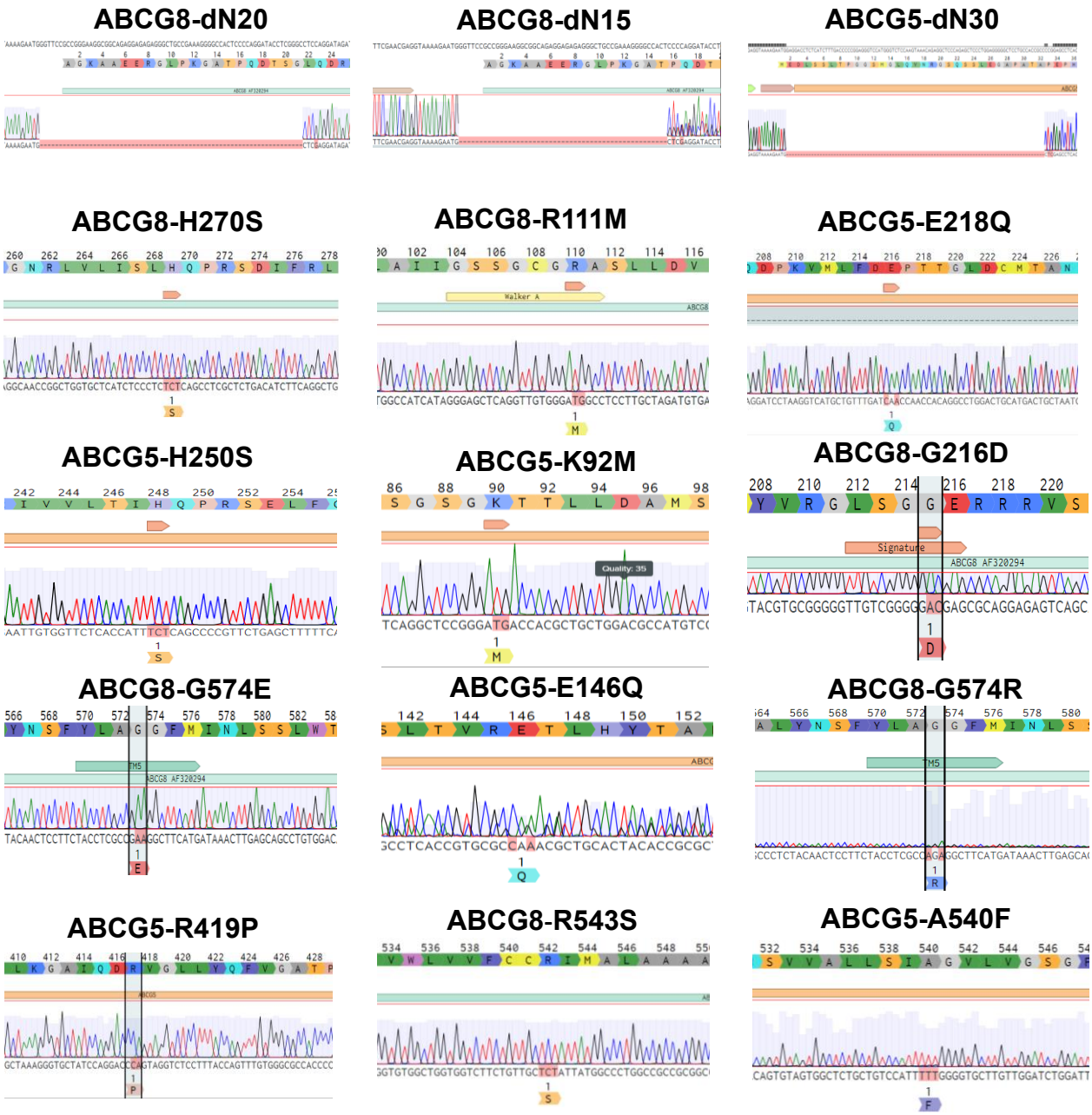

Figure 3. 5: Sequencing results.

This figure shows the sequencing results after the mutagenesis. The sequencing results show the three successful deletions at the N terminal of both genes and amino acid substitution in all disease and catalytic mutants. The Sanger sequencing was performed by Eurofins Genomics Canada.

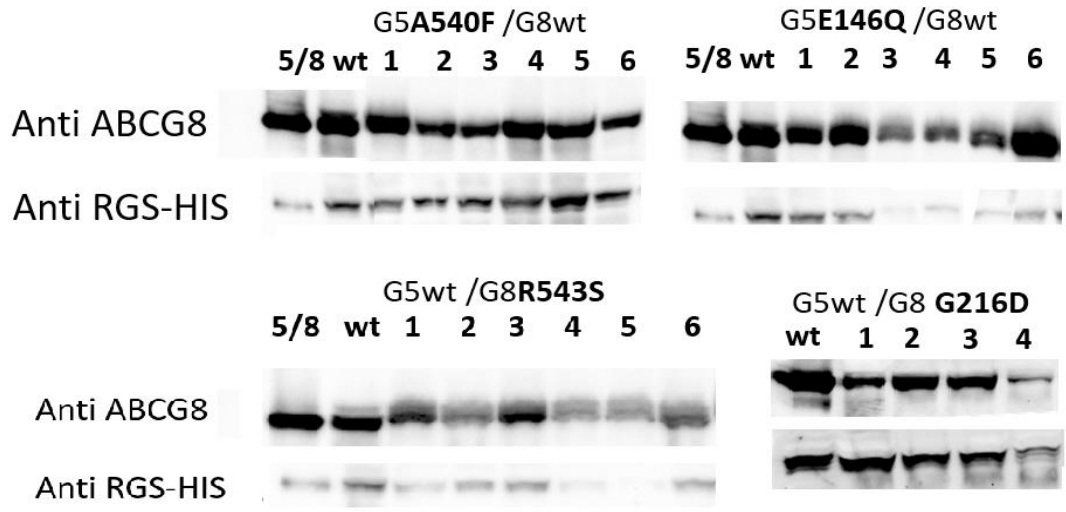

Figure 3. 6: Expression analysis of different ABCG5/G8 mutants.

Crude microsomal membranes, containing 20-30µg total proteins, were resolved by SDS–PAGE. Protein expression was analyzed by immunoblotting using monoclonal anti-RGSH4 antibodies to detect ABCG5 and polyclonal anti-hABCG8 antibodies to detect ABCG8**.** The clones expressing the highest levels of both subunits were selected and stored in 15–20% glycerol at −80 °C.

3.2 Optimization of expressing ABCG5/G8 mutants

The initial expression tests revealed that the expression protocol used for wild type ABCG5/G8 does not yield satisfactory expression of the ABCG5/G8 mutants. For several membrane proteins and their mutants, higher and more stable expression was observed when induced at different temperatures (Huang et al., 2008; Tanapongpipat et al., 2012; André et al., 2006). To test if the maturation of ABCG5/G8 mutants at different temperatures, the protein expression was induced at 20°C or 25°C as opposed to induction at 30°C as described in section 2.2.4. The cells were disrupted to make crude membranes, which were run on 10% SDS-PAGE gels, and protein expression was analyzed by immunoblotting using anti-RGSH4 antibodies to detect ABCG5 and anti-hABCG8 antibodies to detect ABCG8. The induction at 20°C showed the best protein expression compared to the other two temperatures (Fig. 3.5). Because a lower temperature would slow down the yeast metabolism, the maximal expression at 20°C was expected to be shifted for few additional hours. Therefore, the cells were harvested 48-60 hours postinduction as opposed to 36-48 hours at 30°C.

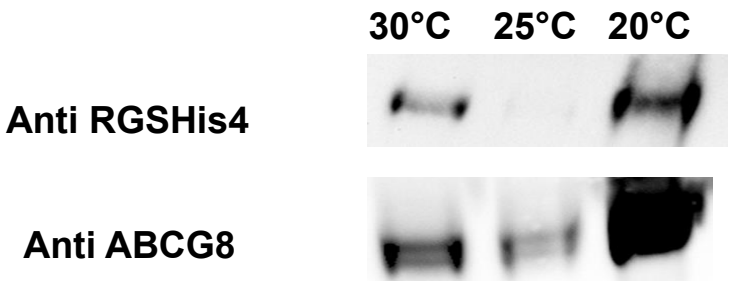

Figure 3. 7: Optimal temperature for mutant ABCG5/G8 expression.

Immunoblotting using anti-RGSH4 anti-hABCG8 antibodies of the crude membranes isolated from cells induced at 20°C, 25°C, and 30°C. 20°C is the optimal temperature.

3.3 Protein purification

3.3.1 WT ABCG5/G8 purification

As described in section 2.1.1, two different constructs were used to purify WT ABCG5/G8. The difference between these constructs is the presence or absence of the CBP tag on ABCG8. So, the purification of the expressed protein was different dependent on the construct used. The expressed protein from the construct lacking the CBP tag goes through one affinity column NI-NTA opposes to two affinity columns with the other. The Ni-NTA column is always the first purification step.

Cells expressing WT ABCG5/G8 were grown and induced as described in sections 2.2.5. After 36-48 hours of induction, the cells were harvested, lysed in emulsifier and microsomes were prepared. The concentration of the total protein content was then measured using the Bradford assay. The total protein concentration obtained was on average 12 ± 3 mg per 200mL. Microsomes were solubilized with 1% DDM and spun down to separate the insoluble materials. The supernatant containing the soluble protein was collected for protein purification. To purify WT ABCG5/G8, the DDM-soluble proteins were applied to the first affinity column (Ni-NTA), following the protocol described in 2.2.8b and the protein was eluted with 200mM imidazole. The collected fractions were applied to a CBP column and the elution fractions were collected for further purification steps. The partially purified WT ABCG5/G8 was then applied to the anion exchanger,

diethylaminoethyl (DEAE). This purification step was newly introduced to WT ABCG5/G8 published protocol to increase its purity and the homogeneity which is very critical for performing structural studies. The partially purified protein was switched to a different buffer before it was applied to the DEAE column as described in section 2.2.8c, then it was eluted with 175mM NaCl. The final purification step was size exclusion chromatography (SEC). The protein was injected through Superdex 200 column and collected and stored for future use. Samples from every purification step were then loaded on 10% SDS PAGE as shown in figure 3.6 for ABCG5/G8 with both tags while figure 3.7 ABCG5G8 with CBP tag only.

The yield of the protein was in a range 5-10mg per 6L of cells (~240g cells). It was concentrated to 1 mg/mL using a 100kDa cut- off concentrator immediately after the size exclusion chromatography step. The solubilization efficiency using 1% DDM was within a range of 25-50% as shown in immunoblot (Fig. 3.7B) and the purity of the protein was higher than 95%. The SEC results showed a single peak appears between 11 and 12mL retention volume with void volume ~8.6 mL (Figure 3.8). the purified WT ABCG5/G8 was mostly homogenous with no large aggregates present, with very low peak at the void volume and a symmetrical shape of elution peak. For functional studies (Chapter 4), we did not observe difference in the ATPase activity of proteins purified with and without the additional DEAE step.

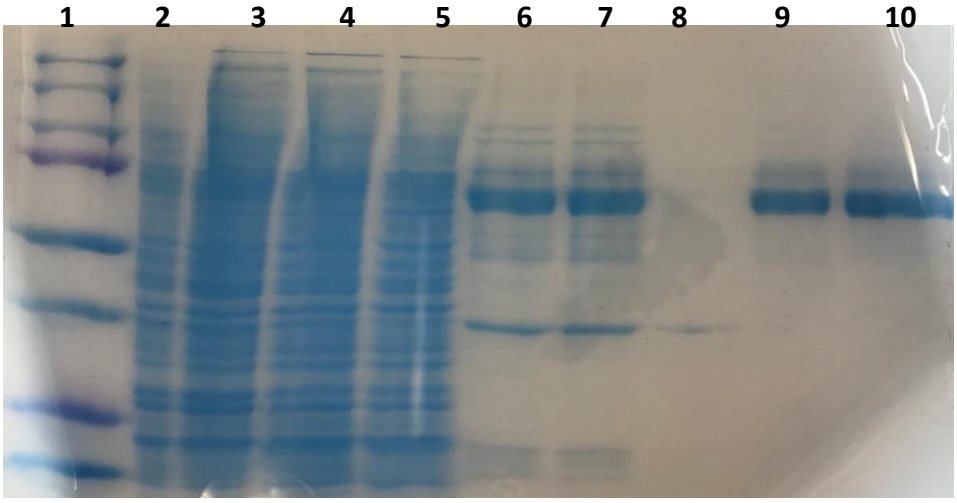

Figure 3. 9: Purification profile of WT ABCG5/G8 with both RGSHis6GH6 and CBP tags.

Protein was expressed in *P. pastoris* and purified by affinity chromatography. The gel was stained with Coomassie blue. Lane 1, molecular mass standard; lane 2, 20 µL of the microsomes; lane 3, 20 µL of the solubilized fraction; lane 4, 20µL of Ni column flow through; lane 5, 20µL Ni column wash with 25mM imidazole; lane 6-7, 10ul of the pooled fractions of Ni column elution; lane 8, 20µL CBP column wash; Lane 9-10, 10ul of the pooled fractions of CBP column elution.

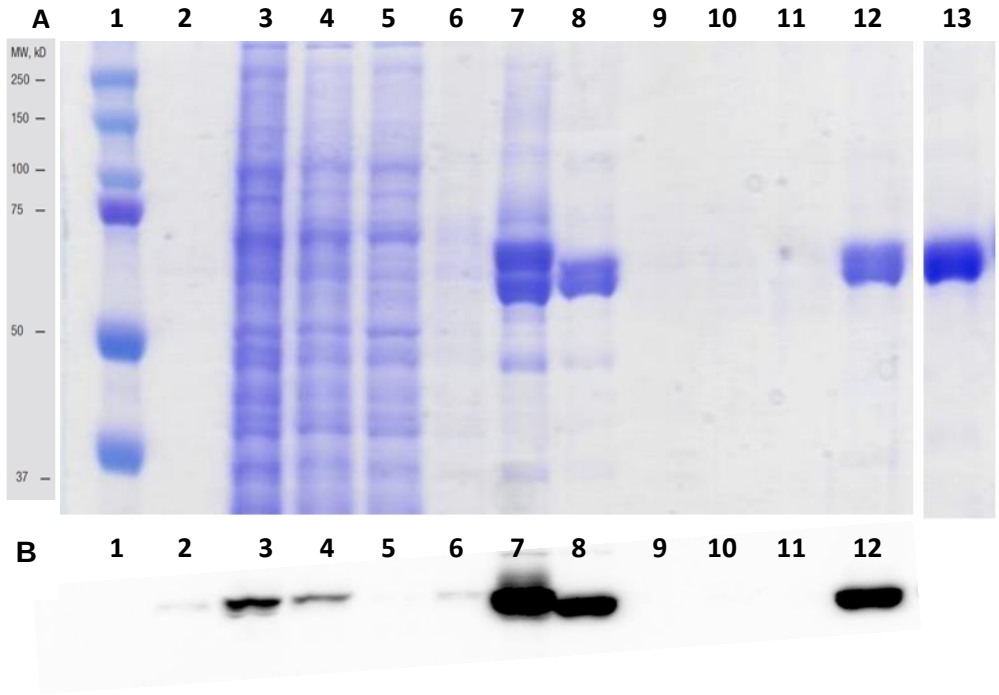

Figure 3. 10: Purification profile of ABCG5/G8 with only RGSHis6GH6 tag.

The protein was expressed in *P. pastoris* purified by tandem affinity chromatography ± Ion exchange, which was followed by size exclusion chromatography (Superdex 200 increase column) the gel was stained with Coomassie blue. (B) Immunoblot using anti-ABCG5 showing the solubilization efficiency using 1% DDM was in the range of 25-50% comparing lane 3 and 4. Lane 1, molecular mass standard; lane 3, 15 µL of the microsomes; lane 4, 15 µL of the solubilized fraction; lane 5, 15µL of Ni column flow through; lane 6, 15µL Ni column wash with 50mM imidazole; lane 7, 15ul of the pooled fractions of Ni column elution ; Lane 8, 15ul of the pooled fractions of Ni fractions treated with Endo H; lane 9, 15ul of the pooled fractions of DAEA resins flow through ; Lane 10, 15ul of the pooled fractions of Ion exchange wash with Buffer E. Lane 11, 15ul of the pooled fractions of Ion exchange wash with buffer E with 50 mM NaCl. Lane 12, 15ul of Ion exchange Eluted fractions with Buffer E with 175mM NaCl; Lane 13, 15ul of the pooled fractions of gel filtration

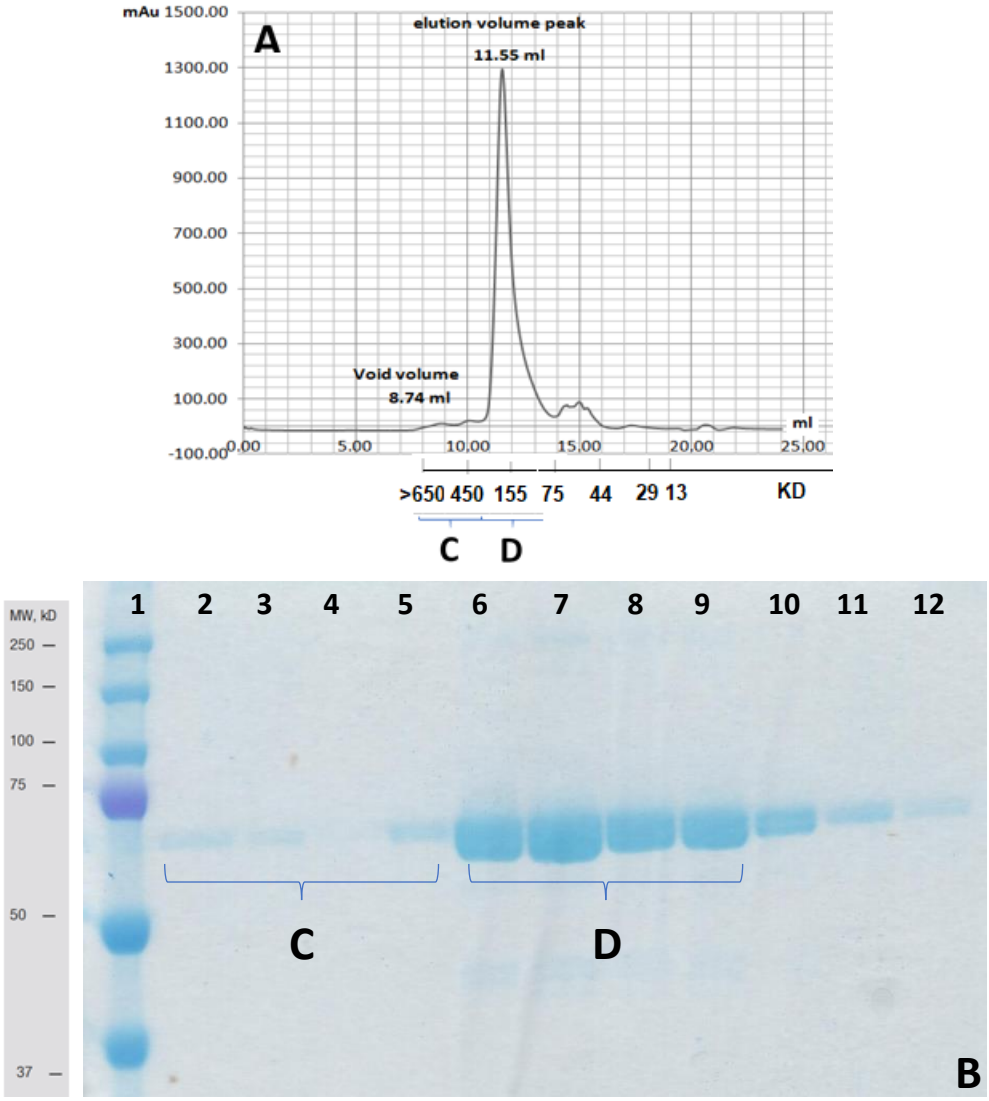

Figure 3. 12: Gel filtration chromatography of WT ABCG5/G8.

Coomassie stained bands visualized on a 10% SDS-PAGE gel. **A:** The elution profile of the ABCG5/G8, the peak of the eluted ABCG5/G8 (D) was shown at 11.55ml while the void volume contains mostly ABCG5/G8 aggregates (C). **B:** The gel shows the ABCG5/G8 band in different fractions collected from gel filtration.

3.3.2 Purification of ABCG5/G8 missense and catalytic mutations

As described in Chapter 2, seventeen constructs with different missense and catalytic mutations were created. Ten of the mutants were catalytic deficient constructs of ABCG5/G8, these mutants produces a cassette that can bind but not efficiently hydrolyze, including the catalytic glutamate to glutamine (G5-E218Q and G8-E238Q), histidine to serine (G5-H250S and G8-H270S), glycine to aspartate (G5-G196D and G8-G216D) and lysine or arginine to methionine (G5-K92M and G8-R111M) (Moody et al., 2002). These mutants are canonically ATPase deficient mutants, and G8-G216D or G5-K92M served as a negative control in the ATPase assays. Other mutants will be used for future structural work for the attempt to determine an atomic model of ATP-bound state of ABCG5/G8. The other 7 constructs, the sterol binding mutation A540F, in addition to the six disease mutants were created to study their impact on ABCG5/G8 function by in vitro assays.

Most of the 17 mutants were expressed and purified as shown in (Figures 3.9-3.11). For my project, I focused on using four of the mutants for ATPase studies (Chapter 4), including the two disease mutants (ABCG5-E146Q and ABC-G8R543S) which are located on the triple helical and polar relay motifs respectively, the canonically dead mutant (ABCG-G8G216D) and the putative sterol binding ABCG5-A540F mutant.

Mutant proteins were expressed and purified using the protocol established for WT proteins described above with minor modification. *P. pastoris* cells were grown in the presence of 1% glycerol for a few days at 30°C. As soon as all glycerol was metabolized, the temperature was reduced to 20°C, 6 hours later cells were fed with 0.5% methanol, and every 12 hours for 48 hours to induce the ABCG5/G8 protein expression. The cells were harvested and resuspended with buffer A. The average weight of the cell pellet was 55 ± 5 g per liter culture which is significantly higher than average of the WT.

The cells were lysed by emulsifier, and by sequential centrifugations, the microsomal membrane was separated from the other organelles and cellular debris. The concentration of the total protein content was estimated using the Bradford assay. The microsomal membranes were then solubilized by 1% DDM with efficiency range of 10-20% which is significantly lower compared with WT (Fig 3.10E). The soluble material was then passed through tandem affinity chromatography, first the protein was passed through a Ni-NTA column, the collected flow through showed some unbound protein, in addition to that, some protein was lost as well during the imidazole washes (25mM and 50 mM) (Fig. 3.10E). This suggests that the binding to the nickel resin was not as strong compared to WT. The protein was then passed through a CBP column. The elution fractions were further purified by size exclusion chromatography using a Superdex

200 Increase column. The eluates were stored at -80 °C in 50-100ul aliquots at a concentration of 0.5-1mg/ml.

The protein yield of the mutants was lower compared to WT, in a range of 400-800µg per six liters of cells (~300g) but sufficient for ATPase assays (Fig 3.11A). Many factors might be the reason of this lower yield. The solubilization efficiency was slightly low (Fig 3.10E). In addition, some protein was lost during Ni-NTA binding and imidazole wash. The profile of the size exclusion chromatography showed a higher peak at the void volume than dimeric proteins, suggesting that the mutant proteins are more prone to aggregation (Fig 3.11A).

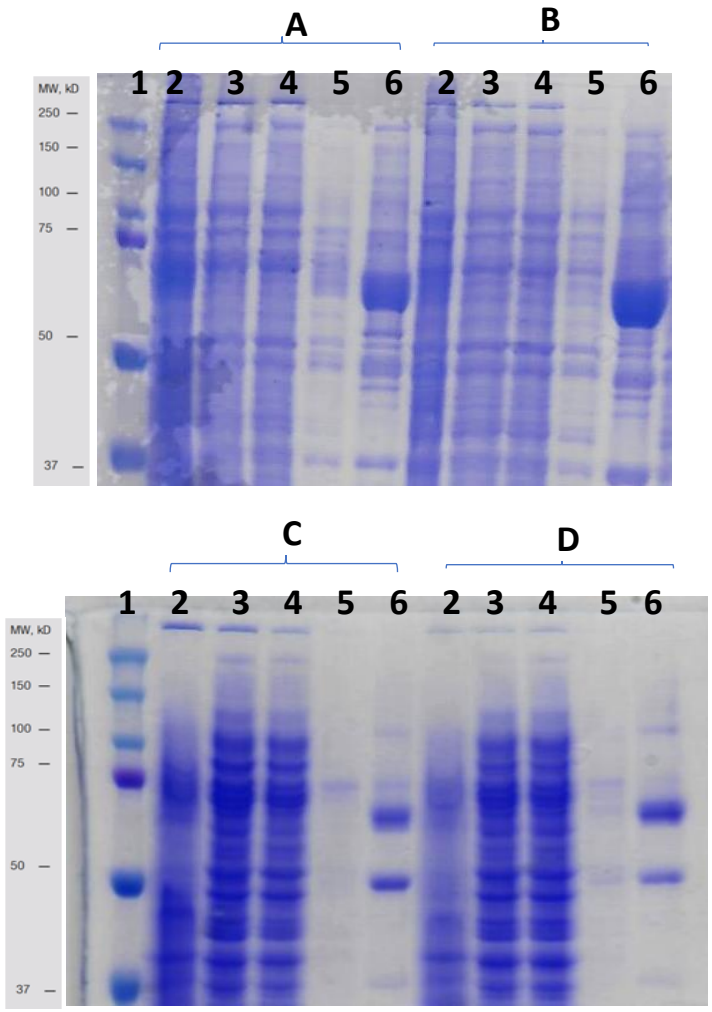

Figure 3. 14: Purification of catalytic mutations of ABCG5/G8

(RGSH6GH6/CBP tags**).** The purification was performed as described in Chapter 2. **A**: Purification profile of ABCG5-H250S/G8 mutant. **B**: Purification profile of ABCG5/G8-E238Q mutant. **C**: Purification profile of ABCG5-E218Q/G8 mutant. **D**: Purification profile of ABCG5/G8-H270S mutant. **E**: Purification profile of ABCG5-K92M/G8 mutant. The following fractions were analyzed by 10% SDS/PAGE and Coomassie dye. Lane 1, molecular mass standard; lane 2, 10 ul of the solubilized fraction; lane 3, 10ul of Ni column flow through; lane 4, 10 ul Ni column wash with 50mM imidazole; lane 5, 10ul of the pooled fractions of Ni column elution ; Lane 6, 15ul of the pooled fractions of CBP column elution.

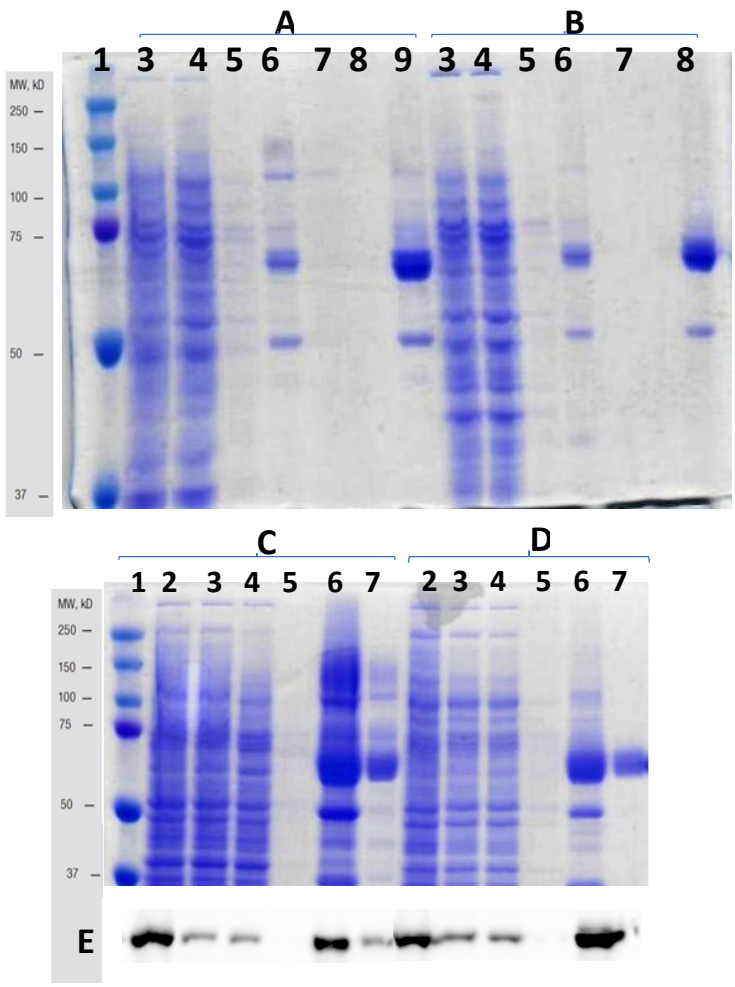

Figure 3. 16: Purification of missense mutations of ABCG5/G8

(RGSH6GH6/CBP tags**).** The purification was performed as described in chapter 2. **A**: Purification profile of ABCG5-E146Q/G8 mutant. **B**: Purification profile of ABCG5/G8-R543S mutant. **C**: Purification profile of ABCG5-A540F/G8 mutant. **D**: Purification profile of ABCG5/G8-G216D mutant. The following fractions were analyzed by 10% SDS/PAGE and Coomassie dye. Lane 1, molecular mass standard; lane 2, 15 ul of the solubilized fraction; lane 3, 15ul of Ni column flow through; lane 4, 15 ul Ni column wash with 50mM imidazole; lane 5, 15ul of the pooled fractions of Ni column elution ; Lane 6, 15ul of the pooled fractions of CBP column elution. **E:** Immunoblot using anti-ABCG5 showing the solubilization efficiency using 1% DDM was in a range of 10-20% comparing lane 2 and 3.

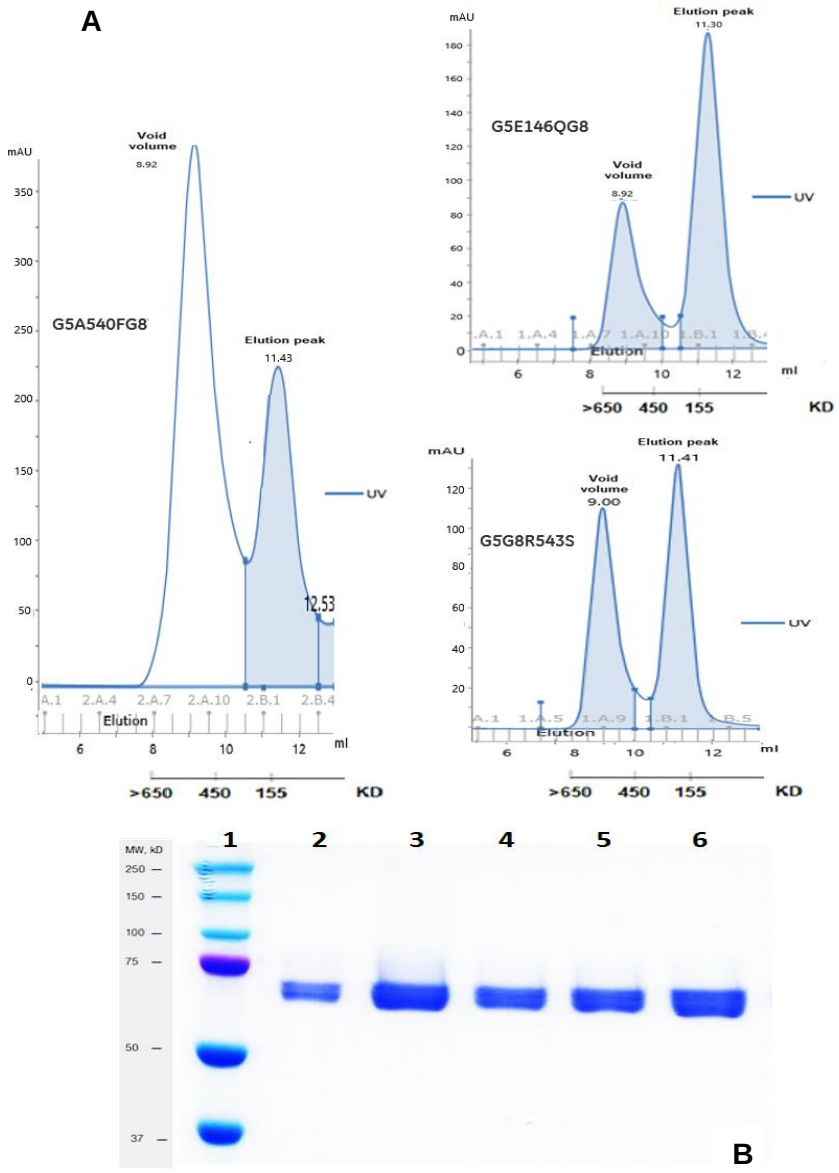

Figure 3. 18: The final product of the purified mutants

(A) The profile of the size exclusion chromatography showed the mutants eluted at the same volume as compared to the WT, proving the proper maturation of mutant's dimer, but a higher peak at the void volume, suggesting that the mutants' proteins are more prone to aggregation. **(B)** The final products of gel filtration chromatography of the mutants G216D 2, E146Q 3, R543S 4, and A540F 5 along with WT ABCG5G8 6. Coomassie stained bands visualized on a 10% SDS-PAGE gel.

3.3.3 Purification of truncated ABCG5/G8

A series of truncated ABCG5/G8 mutants were created by removing several amino acids at the N termini of both ABCG5 and ABCG8 as described in section 2.2.1. The deleted segments represent unresolved segments in the published ABCG5/G8 atomic model (Lee et al., 2016). These constructs were created for future structural work to solve the ABCG5/G8 model at a higher resolution. The different truncated proteins were expressed and purified as follows:

The cells expressing the truncated protein were cultured similar to WT as described above. The membrane proteins were prepared the same way as described section 2.2. The microsomes were solubilized and purified by the two-affinity column, Ni-NTA and CBP in addition to size exclusion chromatography. The yield of the protein was in a range similar to WT ABCG5/G8 or 4-6 mg per 6L of cells (~240g cells). The purity of the protein was as shown in Fig. 3.12. The size exclusion chromatography resulted in a single peak between 11 and 12mL retention volume with void volume (~8.6 mL). Like the purified WT, the truncated ABCG5/G8 was mostly homogenous with no large aggregates present and a very minor peak at the void volume.

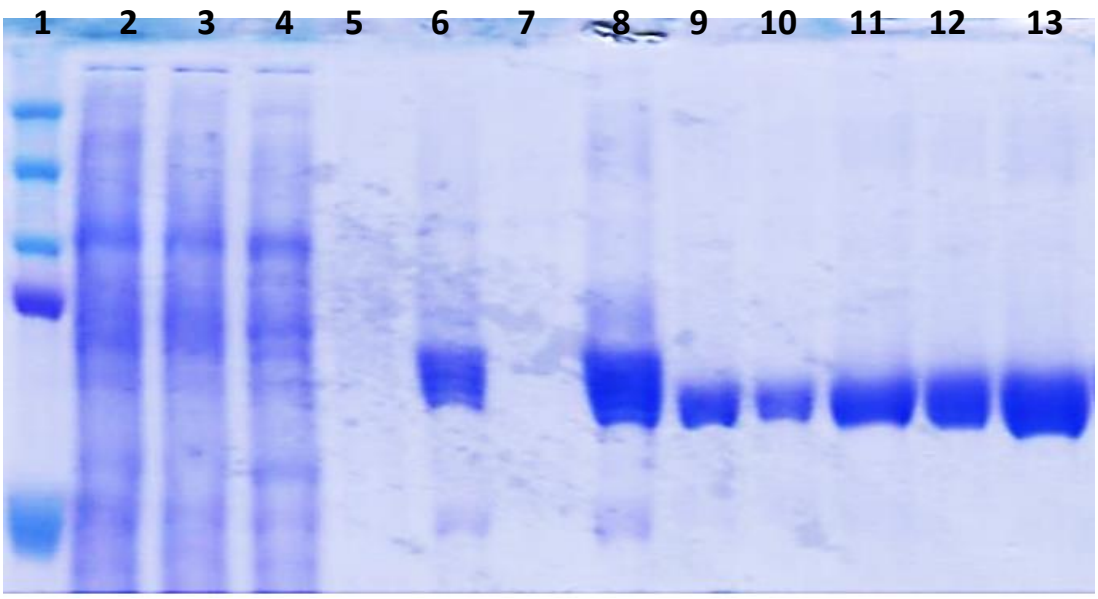

Figure 3. 12: Purification profile of the truncated ABCG5/G8-dN15. (RGSH6GH6/CBP tags). The purification was performed as described in chapter 2. The following fractions were analyzed by 10% SDS/PAGE and Coomassie dye. Lane 1, molecular mass standard; lane 2, 15 µL of the microsomes; lane 3, 15 µL of the solubilized fraction; lane 4, 15µL of Ni column flow through; lane 5, 15µL Ni column wash with 50mM imidazole; lane 6, 10ul of the pooled fractions of Ni column elution; lane 7, 15µL CBP column wash; Lane 8, 15ul of the pooled fractions of CBP column elution; Lane 9, 15ul of the pooled fractions of CBP elution treated with Endo H; Lane 10-13, 15ul of the pooled fractions of gel filtration.

Chapter 4 Results - ATPase Activity of Missense Mutations of ABCG5/G8

4.0 Rationale:

In order to further define the mechanism of ABCG5/G8-mediated sterol transport, additional information is required. Therefore, the effect of missense loss-of-function disease mutations (mapping to locations near or within the various conserved structural motifs, Figure 1.4) on ATPase activity was assessed. This information can contribute to establishing the transport mechanism of ABCG5/G8.

4.1 CHS-coupled ATPase activity of WT ABCG5/G8

The protein concentrations were determined prior to starting the ATP assays. Samples of 5µL of each WT and mutants ABCG5/G8 proteins were separated on a 10% SDS PAGE along with known BSA concentrations. The intensities of the bands were then quantified by Image-J, and the concentration of the different proteins were determined. The concentration of the proteins was estimated as follow: WT ABCG5/G8 of 0.7 µg/µL, ABCG5-A540F/G8 of 0.4 µg/µL, ABCG5-E146Q/G8 of 0.5µg/µL, ABCG5/G8-R543S of 0.4µg/µL, and ABCG5/G8-G216D of 0.6µg/µL. The volume of the protein sample added to each ATPase

reaction was then adjusted such that exactly 3.5µg of protein was added to each reaction.

The detergent-purified WT ABCG5/G8 was incubated in the presence of 2.6mM *E. coli* polar lipids, 1.5% sodium cholate, 10mM sodium azide (a known inhibitor of F1-ATPase which could be copurified with our proteins), and with or without 4.1mM CHS. The reactions were all set up at room temperature, then the protein-lipid mix was incubated for 10 minutes at 37°C, before initiating the reaction by adding 5x ATP cocktail then 8.6µL was quenched out at different time point over 60 minutes, as it was described in section 2.2.9. After quenching the reaction at different time points, the released inorganic phosphate was monitored, and the results showed that the hydrolysis of ATP was increased linearly in the first 12 minutes and subsequently reached an equilibrium (due to the accumulation of ADP). Hence, the rate of the hydrolysis was measured between 0 and 12 minutes in all the experiments. The basal activity of WT ABCG5/G8 measured in the presence of *E. coli* lipids supplemented with 1.5% sodium cholate was 160 ± 15 nmol min^{-1} mg^{-1}. The activity was stimulated by 3.52 folds to 565 ± 30 nmol min^{-1} mg^{-1} with addition of 4.1mM CHS (Fig. 4.1 A B). ATPase-deficient mutant ABCG5/G8-G216D was reconstituted in the lipids mix the same as WT but its activity was completely abolished in presence or absence of CHS (Fig. 4.1 A B). Hence, this mutant was used as negative control along with all experiments.

4.2 CHS-coupled ATPase activity of mutants ABCG5/G8

The detergent purified mutants were incubated in *E. coli* lipids following the same procedure as WT. The loss-of-function missense mutants ABCG5-E146Q/G8WT and ABCG5WT/G8-R543S has shown a reduction of CHS-coupled ATP hydrolysis, but retain ~20% activity as compared to WT, 160 ± 15 nmol min^{-1} mg^{-1} and 150 ± 5 nmol min^{-1} mg^{-1} respectively. While the putative sterol binding mutant ABCG5-A540F/G8WT has shown further reduction in the ATPase activity to ~10% of WT, 90 ± 10 nmol min^{-1} mg^{-1} (Fig. 4.1 C).

4.3 ABCG5/G8 ATPase activity depends on concentration of CHS.

The effects of CHS on ABCG5/G8 WT and mutants were further investigated by measuring the ATP hydrolysis in the presence of different concentrations of CHS and a saturating concentration of ATP (5mM).WT ABCG5/G8 became saturated at 2.5mM ATP, so to hydrolyze 2.5mM ATP, the protein reaches it maximum activity and above this concentration the protein is saturated. As described above, proteins were preincubated with *E. coli* polar lipids, sodium cholate and a wide range of CHS concentrations (0.064 mM – 4.1mM). Figure 4.2 shows the CHS-coupled ATPase activity in a concentration dependent manner with maximal activity occurring at ~4.1mM CHS. The half maximal activity at 0.7mM for WT was

similar to AGBG5-A540F/G8 of 0.699, while the half maximal activity of the disease mutants was significantly higher than WT, ABCG5-E146Q of 1.26 mM CHS and ABCG8-R543S of 2.3 mM CHS. The turnover rate k_{cat} of the WT and the mutants were calculated using the formula $V_{max} = k_{cat} \times [E]$, where Vmax is the ATP hydrolysis rate (nmol min^{-1} mg^{-1}), k_{cat} is the turnover rate (S^{-1}) and [E] is the concentration of enzyme (µM). The concentration of the protein used in every reaction was 3.5 µg with Molecular weight of 148183 g/mol and the reaction volume was $65x10^{-6}$ L. The k_{cat} of the protein was divided by its K_M to calculate the protein catalytic efficiency. The calculated k_{cat} and k_{cat}/K_M and Gibbs free energy lost from WT to each mutant (DDG_{MUT}) were calculated and listed in the table (Fig. 4.2).

4.4 Enzymatic parameters of ATP hydrolysis by ABCG5/G8 WT and mutants.

To examine the CHS-coupled ATPase activity at different ATP concentrations, the purified protein was preincubated with *E. coli* polar lipids, sodium cholate, and 4.1mM CHS, then ATP hydrolysis was initiated with different concentrations of ATP (0.15mM-5mM). The maximum activity of different protein was observed at or above 2.5mM ATP with a V_{max} of 677 ± 50 nmol min^{-1} mg^{-1} for WT ABCG5/G8, V_{max} of 101 ±10 nmol min^{-1} mg^{-1} for ABCG5-A540F/G8, V_{max} of 167 ±10 nmol min^{-}

^{1} mg^{-1} for ABCG5-E146Q/G8, and V_{max} of 150±10 nmol min^{-1} mg^{-1} for ABCG5/G8-R543S. A same K_M (ATP) of ~0.5mM was obtained for WT and mutants (Fig. 4.3). The ATP turnover rate k_{cat} of the WT and the mutants were calculated using the formula $V_{max} = k_{cat} \times [E]$, where V_{max} is the ATP hydrolysis rate (min^{-1} mg^{-1}), k_{cat} is the ATP turnover rate (S^{-1}) and [E] is the concentration of enzyme (µM). Similar to the different CHS concentration experiment, the same reaction setup was used, the concentration of the protein used in every reaction was 3.5 µg with Molecular weight of 148183 g/mol and the reaction volume was $65x10^{-6}$ L.

The WT ATP turnover was 1.74 S^{-1}, this means almost every second, WT ABCG5/G8 can hydrolyze two ATP molecules. The mutant's turnover of the ATP was reduced significantly as shown in the table (Fig. 4.3). ABCG5-A540F mutant requires 4 seconds to turnover one molecule of ATP, while it takes 2.5 second with both disease mutants ABCG8-R543S and ABCG5-E146Q mutants. The k_{cat} of the protein was divided by its K_m to calculate the protein catalytic efficiency, and Gibbs free energy lost from WT to each mutant (DDG_{MUT}) are listed in the table (Fig. 4.3).

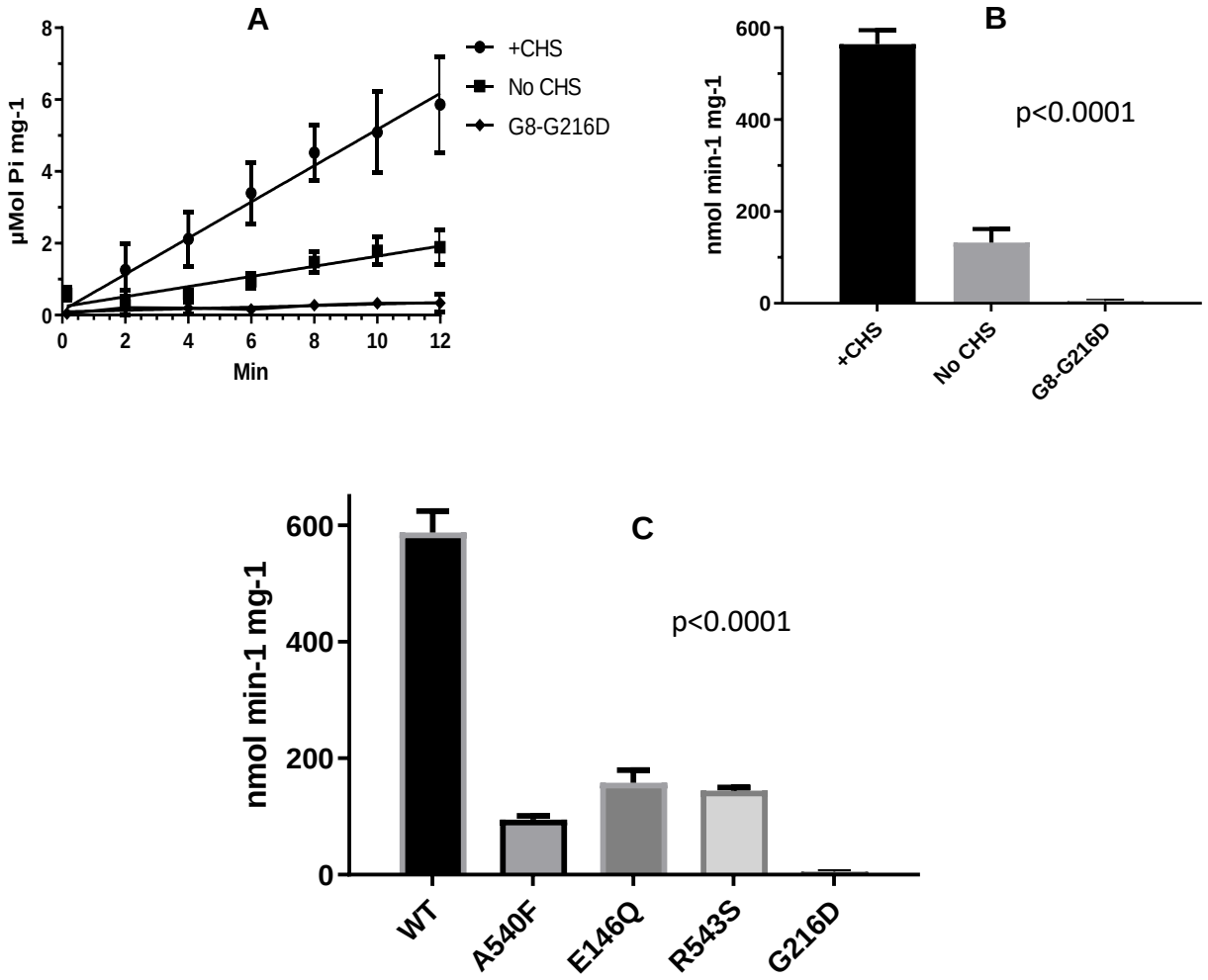

Figure 4. 1: ATPase activity of ABCG5/G8.

The detergent purified protein was incubated with E. coli lipids, sodium cholate in presence or absence of 4.1 mM CHS. the assay was initiated by addition of 5mM ATP, 7.5mM $MgCl_2$ and 10mM sodium azide at 37°C. the reaction was stopped at different time points and the amount of inorganic phosphate was measured as described in section 2.2.9. **A:** The average values from 6 different independents experiments at different time points (key above). The bar graph of the mean values obtained from at least four different experiments **(B)** shows the effect of CHS on the basal specific Activity of ABCG5/G8, while **(C)** shows the effect of the mutants on the specific activity of CHS stimulated ATPase activity.

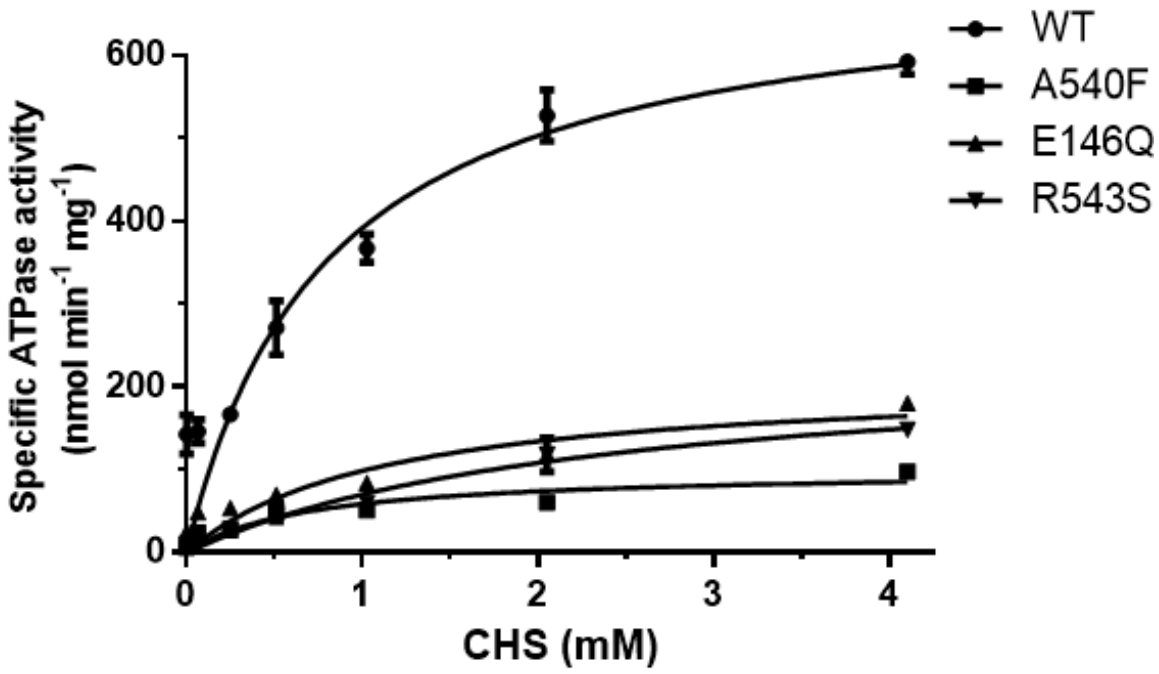

	V_{max} (nmol/min/mg)	K_M (CHS) (mM)	k_{cat} (s^{-1})	k_{cat}/K_M (M^{-1} s^{-1})	DDG_{MUT} (kJ/mol)
WT	702.9 ± 50.7	0.8	1.74	$2.2x10^3$	-
G5-E146Q	210.0 ± 33.2	1.13	0.52	$0.46x10^3$	10
G8-R543S	237.1 ± 33.4	2.38	0.59	$0.25x10^3$	9
G5-A540F	99.8 ± 11.4	0.70	0.25	$0.36x10^3$	16.1

Figure 4. 2: CHS-dependent ATPase activity of purified WT ABCG5/G8 and three missense mutants.

(key showing above) Purified protein with lipid mixes in presence of various concentrations of CHS. The Michaelis-Menten equation was fitted to the experimental data, and the determined V_{max}, K_M, k_{cat}, k_{cat}/K_M and DDG_{mut} are summarized in the tables above.

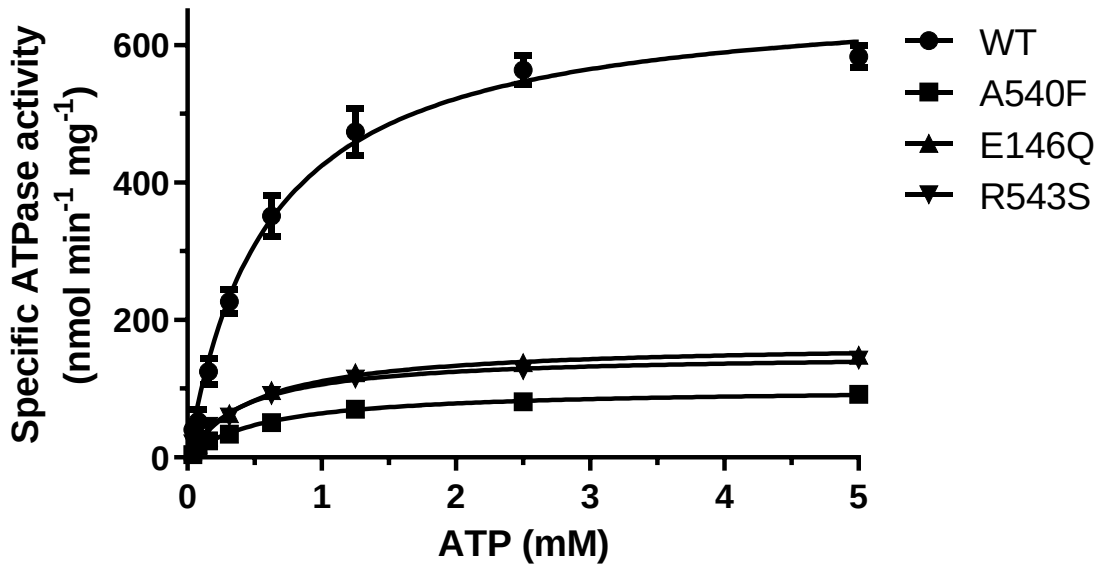

	V_{max} (nmol/min/mg)	K_M (ATP) (mM)	k_{cat} (s^{-1})	k_{cat}/K_M (M^{-1} s^{-1})	DDGMUT (kJ/mol)
WT	677.1 ± 25.6	0.60	1.69	$2.8x10^3$	-
G5-E146Q	167.1 ± 0.05	0.51	0.41	$0.82x10^3$	11.7
G8-R543S	150.7 ± 3.7	0.42	0.38	$0.90x10^3$	12.3
G5-A540F	101.2 ± 4.2	0.58	0.25	$0.43x10^3$	15.8

Figure 4. 3: ATP dependence of purified ABCG5/G8 and mutants.

(key showing above) Purified protein with lipid mix was incubated at 37°C with various concentrations of ATP. The Michaelis-Menten equation was fitted to the experimental data, and the determined V_{max}, K_M, k_{cat}, k_{cat}/K_M and DDG_{mut} are summarized in the tables above.

4.5 Effect of sterols on ABCG5/G8 ATPase activity.

The ATPase assays were carried out in the presence or absence of CHS and were supplemented with different cholesterol or stigmasterol concentrations. Sterols are not soluble in aqueous solutions, hence cholesterol and stigmasterol, used in this study, were dissolved in methyl-β-cyclodextrin (MβCD) at a 1:10 molar ratio as described in section 2.2.8c.

MβCD was tested first to examine if it has any effect on the ATPase assays, so the lipid mix was supplemented with 6.5mM or 13mM of MβCD. The result (Fig. 4.4) revealed that MβCD does not have any effect on the ATP hydrolysis and can be used as very effective tool to dissolve the different sterols used in this study.

Purified ABCG5/G8 was incubated in *E. coli* polar lipids, sodium cholate, 4.1 mM CHS with various concentrations of MβCD-cholesterol or MβCD-stigmasterol, and the activity was measured. A significant decrease of the activity of ABCG5/G8 was observed in concentration-dependent manner and a complete abolished of this activity was obtained at 2.5mM cholesterol or above (Fig. 4.5AB). Interestingly, the inhibitory effect of MβCD-stigmasterol was higher than MβCD-cholesterol effect, as 50% of the reduction of activity by 500μM MβCD-cholesterol was obtained with only 50μM MβCD-stigmasterol. The effect of these two sterols on ABCG5/G8 activity without CHS was the tested. A similar inhibitory effect as that in presence of CHS was obtained (Fig 4.5 CD). The ATPase activity was reduced significantly at 80μM MβCD-stigmasterol while same reduction was

observed at 300μM MβCD-cholesterol. The ATPase activity was completely abolished above 250μM MβCD-stigmasterol and 1.3mM MβCD-cholesterol. Possible interpretation will be discussed in Chapter 5, and further analysis is needed to confirm this observation.

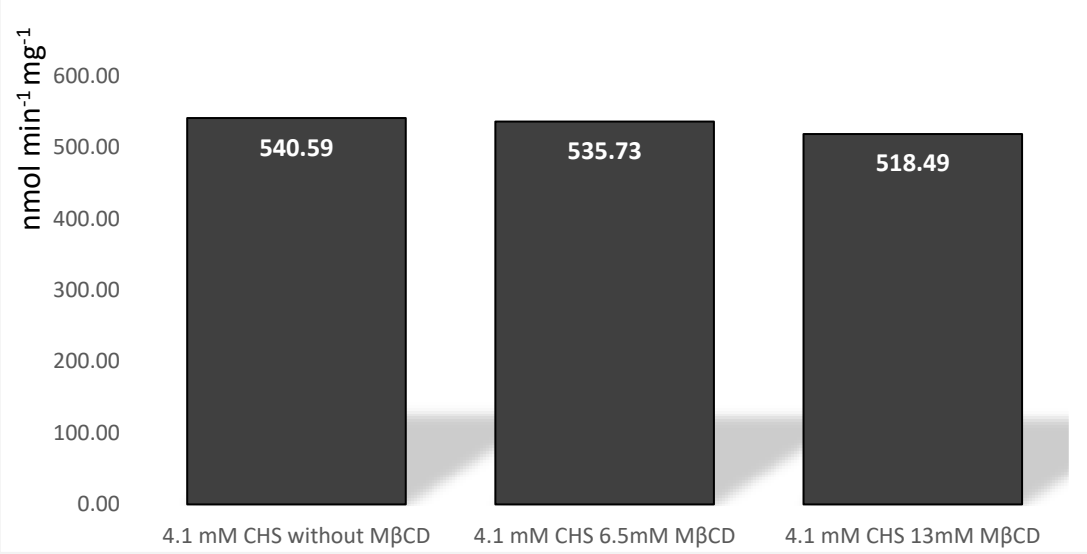

Figure 4. 4: Specific activity of WT ABCG5/G8 in presence of MβCD.

To examine if MβCD has any effect on the ATPase assays, the assay was performed in presence of 13mM MβCD, which is maximum concentration that could be used in the experiments. The specific activity did not show any significant change in presence or absence of MβCD.

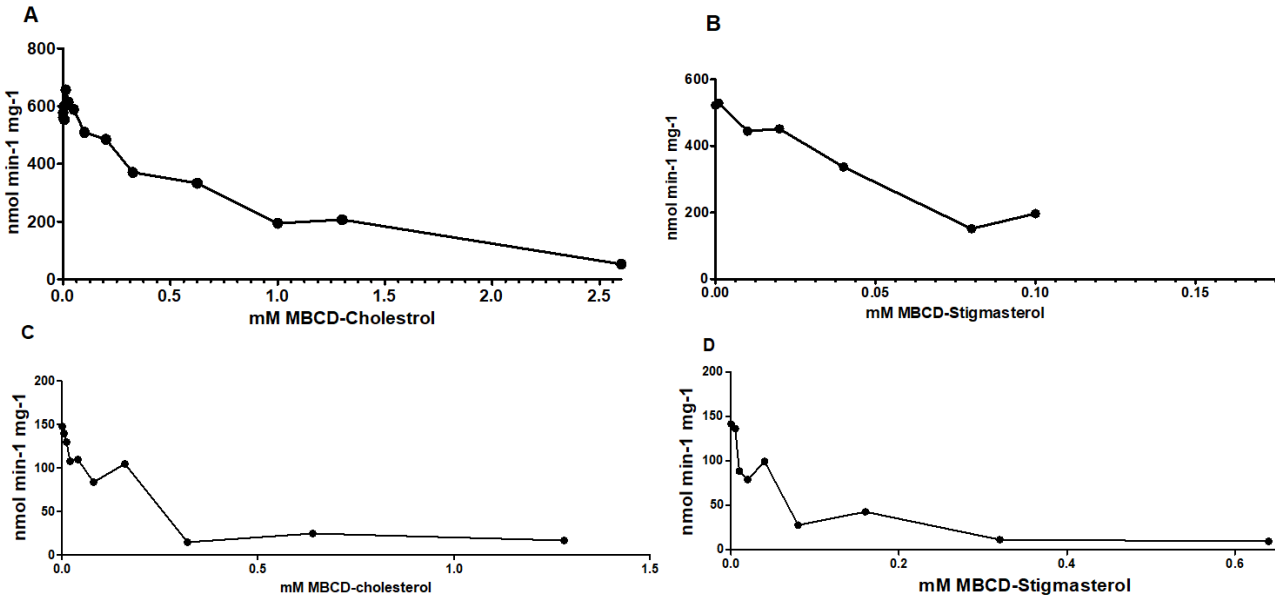

Figure 4. 5: Sterol dependence of ATPase activity.

A: ATPase activity of ABCG5/G8 WT in presence of 4.1mM CHS and various concentration of MβCD-cholesterol. **B**: ATPase activity of ABCG5/G8 WT in presence of 4.1mM CHS and various concentration of MβCD-stigmasterol. **C**: ATPase activity of ABCG5/G8 WT in absence of CHS and various concentration of MβCD-cholesterol. **D**: ATPase activity of ABCG5/G8 WT in absence of CHS and various concentration of MβCD-stigmasterol.

Chapter 5 General Discussion and Conclusion

By mapping the residues that carry sitosterolemia mutations on the apo structure of ABCG5/G8 (Zein et al., 2019), we have found that the majority of missense variants occur within or near a structural motif, which are believed to play important roles in ABCG5/G8 functions. Several missense mutations (ER-trapped) prevent protein maturation from the ER, but at least five mutations (ER-escaped) have been shown to undergo proper trafficking to post-ER cell membranes (Graf et al., 2004). So far, no study has been reported to show the impact of these ER-escaped missense mutants on ABCG5/G8 function using either *in vitro* or *in vivo* models. While it is possible to use transgenic mouse models to test these mutants *in vivo*, it is not clear to us that such study would reveal the mechanistic details of ABCG5/G8 and the effects from the mutants. Therefore, in order to establish its mechanistic basis, it was essential to use a purified system to investigate the functional activity of ABCG5/G8 *in vitro* and to analyze the structure-function relationship of such sterol transporter.

To facilitate these goals, I began by engineering a series of ABCG5/G8 variants (Chapter 2), including catalytically deficient mutants, ER-escaped disease-causing mutants, and truncated mutants that removed the disordered N-termini. In this thesis, I have cloned, sequenced, transformed the mutant constructs into *P. pastoris*, and expressed a total of 17 catalytical and disease-

causing ABCG5/G8. Four of these constructs were selected for further expression analysis and larger-scale purification for this thesis research. The results of this work have shown that all of the mutants can be expressed in *Pichia pastoris* yeast and all constructs can undergo protein maturation as the WT. The reagents established here will be beneficial to biochemical and structural studies of this important ATP transporter in cholesterol homeostasis and lipid metabolism.

5.1 Expression and purification of ABCG5/G8 missense mutants.

The initial attempt to purify the mutant proteins did not lead to satisfactory yields. Previous studies of other membrane proteins (*e.g.*, G-Protein Coupled Receptor) have shown that low temperature was critical to obtain a significant increase in the expression of functional protein in *P. pastoris* (Andre et al., 2006). It is believed that this change in temperature promoted the expression of chaperones that are needed for membrane protein folding. Here, my work has shown that 20°C is the optimal temperature for proper expression and maturation of ABCG5/G8 disease-mutants. Similar to WT, all the mutants could be purified by the previously described protocol (Lee et al., 2016). As an additional observation, during the purification process, I have noticed that some mutant proteins did not bind tightly to the affinity resins, and they tended to appear as proteins aggregates.

This suggests that reduction of protein stability may contribute to malfunction of ABCG5/G8, subsequently causing diseases.

5.2 ATPase activities of three missense mutants: ABCG5-E146Q, ABCG8-R543S and ABCG5-A540F

Previous *in vivo* studies have shown that defect in ATPase activity of ABCG5/G8 abolished biliary cholesterol secretion. Here I have exploited the ATPase assay as the functional proxy to characterize the activities of purified ABCG5/G8 (WT and mutants). In Chapter 4, I have purified two disease mutants ABCG5-E146Q and ABCG8-R543S, the putative sterol binding ABCG5-A540F mutant, and the catalytically dead mutant ABCG-G8G216D to study the impact of the four mutations on the ATPase activity of ABCG5/G8.

Based on the newly developed ATPase assay in our laboratory, I have determined stimulated ATP hydrolysis by ABCG5/G8 in the presence of cholesteryl hemisuccinate (CHS) (Xavier et al, unpublished). Here, I have performed ATPase assay by using *E. coli* polar lipids (Avanti), a common phospholipid resources to reconstitute ABC transporters in micelles. The basal activity of ABCG5/G8 was 160 ± 15 nmol min-1 mg-1 in the absence of CHS, which is similar to reported values (Johnson et al., 2010). In the presence of CHS, the specific ATPase activity

of ABCG5/G8 was increased ~4-fold to 565 ± 30 nmol min^{-1} mg^{-1} (Fig. 4.2). As the negative control, the G216D mutant displayed no ATPase activity at all.

The loss-of-function missense mutants ABCG5-E146Q/G8WT and ABCG5WT/G8-R543S has shown a reduction of CHS-coupled ATP hydrolysis, but retain ~20% activity as compared to WT, 160 ± 15 nmol min^{-1} mg^{-1} and 150 ± 5 nmol min^{-1} mg^{-1} respectively. While the putative sterol binding mutant ABCG5-A540F/G8WT has shown further reduction in the ATPase activity to ~10% of WT, 90 ± 10 nmol min-1 mg-1 (Fig. 4.2 C). These results support our hypothesis of impaired ATPase activity for the disease-mutants. The ATPase activity remained the same as the basal level, suggesting that these mutant residues may alter the protein conformation to prevent interaction between CHS and the transporter. In the atomic model of ABCG5/G8 (PDB #: 5D07), E146 residue is located on the E-helix of the triple helical bundle and R543 residue is located in the polar relay motif (Fig. 1.6). It is thus possible that these motifs may be directly involved in such ligand-protein interactions. Further studies will reveal better insight of this molecular event. I then characterized the kinetic parameters of CHS-stimulated ATP hydrolysis of these mutants. The K_M values of CHS was significantly increased in the disease mutants compare to WT with decreased ATPase activity (Fig. 4.3), suggesting that CHS is interacting with ABCG5/G8 and regulating the ATPase site remotely. In terms of ATP concentrations, the K_M values of ATP

remain almost the same (4.4), suggesting that ATP binding was not affected by these mutants.

Finally, I studied the effect of the cholesterol and stigmasterol on ABCG5/G8's ATPase activity. Previous *in-vivo* studies suggested sterol selectivity by ABCG5/G8 (Yu et al., 2004). Here, I tested the effect of these two sterols on the ATPase activity of ABCG5/G8 in a wide range of sterol concentrations, 1μM-2mM. The preliminary data showed that in the absence or presence of the sterols, the ATP hydrolysis was inhibited to various extent. Of particular, the CHS stimulated and the basal ATPase activity of the ABCG5/G8 were decreased by concentration dependent manner of cholesterol, and higher sterol concentration almost abolished the ATPase activity. This result suggests more complicated interaction between the proteins and the sterols and requires further studies to interpret the data. The high concentration of these sterols may also have an effect on the lipid composition, thus affect the stability of the protein, or the interaction of the sterols with ABCG5/G8. In addition, we have observed higher inhibitory effect of stigmasterol, compared with cholesterol. Further studies with other sterols and at different sterol concentration may give a better insight into of the sterol specificity of ABCG5/G8.

References

Abdemami, B., Shokrgozar, M. A., Shahreza, H. K., Ghavami, M. (2011). Design and construction of two yeast shuttle vectors containing human procollagen genes expression cassette for expression in yeast. *Avicenna journal of medical biotechnology*, 3(1), 11–18.

André, N., Cherouati, N., Prual, C., Steffan, T., Zeder-Lutz, G., Magnin, T., Reinhart, C. (2006). Enhancing functional production of G protein-coupled receptors in Pichia pastoris to levels required for structural studies via a single expression screen. *Protein science: a publication of the Protein Society*, 15(5), 1115–1126.

Balasubramaniyan, N., Ananthanarayanan, M. and Suchy, F.J. (2016) Nuclear factor-κB regulates the expression of multiple genes encoding liver transport proteins. *Am. J. Physiol. Gastrointest. Liver Physiol.* **310,** G618-628.

Berg JM, Tymoczko JL, Stryer L. Biochemistry. 5th edition. New York: W H Freeman; (2002) Section 4.1, The Purification of Proteins Is an Essential First Step in Understanding Their Function.

Berge, K.E., Tian, H., Graf, G.A., Yu, L., Grishin, N.V., Schultz, J. et al (2000) Accumulation of dietary cholesterol in sitosterolemia caused by mutations in adjacent ABC transporters. *Science* 290, 1771-1775.

Bertheleme N, Singh S, Dowell S. (2015) Bernadette Byrne Heterologous Expression of G-Protein-Coupled Receptors in Yeast. *Methods in Enzymology*. 556, 0076-6879.

Bhattacharyya, A.K. and Connor, W.E. (1974) Beta-sitosterolemia and xanthomatosis. A newly described lipid storage disease in two sisters. *J. Clin. Invest.* 53,1033-1043.

Bloom, D.E., Cafiero, E.T., Jané-Llopis, E., Abrahams-Gessel, S., Bloom, L.R., Fathima, S., et al (2011) The Global Economic Burden of Noncommunicable Diseases. Geneva: World Economic Forum. https://www.weforum.org/reports/global-economic-burden-non-communicable-diseases.

Borst, P. and Elferink, R.O. (2002) Mammalian ABC transporters in Health and Disease. Annu. Rev. *Biochem*. 71, 537-592.

Brown, M. S., Kovanen, P. T., & Goldstein, J. L. (1981). Regulation of plasma cholesterol by lipoprotein receptors. *Science* (New York, N.Y.), 212(4495), 628–635.

Byun, S., Jung, H., Chen, J., Kim, Y.C., Kim, D.H., Kong, B. *et al* (2019) Phosphorylation of hepatic farnesoid X receptor by FGF19 signaling-activated Src maintains cholesterol levels and protects from atherosclerosis. *J. Biol. Chem.* **294,** 8732-8744.

Cariani, L., Thomas, L., Brito, J., & del Castillo, J. R. (2004). Bismuth citrate in the quantification of inorganic phosphate and its utility in the determination of membrane-bound phosphatases. *Analytical biochemistry*, 324(1), 79–83.

Chakrabarti R1, Schutt CE. (2001) The enhancement of PCR amplification by low molecular-weight sulfones. *Gene* 22;274(1-2):293-8.

Chaptal, V., Delolme, F., Kilburg, A., Magnard, S., Montigny, C., Picard, M., Prier, C., Monticelli, L., Bornert, O., Agez, M., Ravaud, S., Orelle, C., Wagner, R.,

Jawhari, A., Broutin, I., Pebay-Peyroula, E., Jault, J. M., Kaback, H. R., le Maire, M., & Falson, P. (2017). Quantification of Detergents Complexed with Membrane Proteins. *Scientific reports*, *7*, 41751.

Dean, M. and Allikmets, R. (1995) Evolution of ATP-binding cassette transporter genes. *Curr. Opin. Genet*. Dev. 5, 779-785.

Dörr, J. M., Scheidelaar, S., Koorengevel, M. C., Dominguez, J. J., Schäfer, M., van Walree, C. A., & Killian, J. A. (2016). The styrene-maleic acid copolymer: a versatile tool in membrane research. European biophysics journal: *EBJ*, 45(1), 3–21.

Fernández FJ, and Vega M.C. (2016) Choose a Suitable Expression Host: A Survey of Available Protein Production Platforms. *Advanced Technologies for Protein Complex Production and Characterization* pp 15-24.

Ford, R.C. and Beis, K. (2019) Learning the ABCs one at a time: structure and mechanism of ABC transporters. *Biochem. Soc. Trans*. 47, 23-36.

Freeman, L.A., Kennedy, A., Wu, J., Bark, S., Remaley, A.T., Santamarina-Fojo, S. *et al* (2004) The orphan nuclear receptor LRH-1 activates the ABCG5/ABCG8 intergenic promoter. *J. Lipid Res.* **45,** 1197–1206.

Frey L; Lakomek NA; Riek R; Bibow S. (2017) Micelles, bicelles, and nanodiscs: comparing the impact of membrane mimetics on membrane protein backbone dynamics. *Angew. Chem. Int. Ed. Engl*. 56, 380–383.

Geisse, S., Gram, H., Kleuser, B., & Kocher, H. P. (1996). Eukaryotic expression systems: a comparison. Protein expression and purification, 8(3), 271–282.

Gómez S, López-Estepa M, Fernández FJ., Suárez T, and Vega M. C. (2016) Alternative Eukaryotic Expression Systems for the Production of Proteins and Protein Complexes. *Advanced Technologies for Protein Complex Production and Characterization* pp 167-184

Graf, G. A., L. Yu, W. P. Li, R. Gerard, P. L. Tuma, J. C. Cohen, and H. H. Hobbs. (2003). ABCG5 and ABCG8 are obligate heterodimers for protein trafficking and biliary cholesterol excretion. *J. Biol. Chem*. 278: 48275-48282.

Graf, G.A., Cohen, J.C. and Hobbs, H.H. (2004) Missense mutations in abcg5 and abcg8 disrupt heterodimerization and trafficking. *J. Biol. Chem*. 279, 24881–24888.

Graf, G.A., Li WP, Gerard RD, Gelissen I, White A, Cohen JC, Hobbs HH. (2002) Coexpression of ATP-binding cassette proteins ABCG5 and ABCG8 permits their transport to the apical surface. *J Clin Invest*, 110(5):659-69.

Graf, G.A., Yu L, Li WP, Gerard R, Tuma PL, Cohen JC, Hobbs HH. (2003) ABCG5 and ABCG8 are obligate heterodimers for protein trafficking and biliary cholesterol excretion. *J Biol Chem*, 278(48): 48275-82.

Grefhorst, A., Verkade, H. J., & Groen, A. K. (2019). The TICE Pathway: Mechanisms and Lipid-Lowering Therapies. Methodist DeBakey cardiovascular journal, 15(1), 70–76.

Harayama, T., Riezman, H. (2018) Understanding the diversity of membrane lipid composition. *Nat Rev Mol Cell Biol* 19, 281–296

Higgins, C. F. (1992) ABC transporters: from microorganisms to man. *Annu Rev Cell Biol*, 8, 67-113.

Hirata, T., Okabe, M., Kobayashi, A., Ueda, K. and Matsuo, M. (2009) Molecular mechanisms of subcellular localization of ABCG5 and ABCG8. *Biosci. Biotechnol. Biochem.* 73, 619-626.

Hirayama, H., Kimura, Y., Kioka, N., Matsuo, M., & Ueda, K. (2013). ATPase activity of human ABCG1 is stimulated by cholesterol and sphingomyelin. *Journal of lipid research*. 54(2), 496–502.

Holland, I. B. & Blight, M. A. (1999) ABC-ATPases, adaptable energy generators fueling transmembrane movement of a variety of molecules in organisms from bacteria to humans. *J Mol Biol*, 293, 381-99.

Holland, I. B. (2011) ABC transporters, mechanisms and biology: an overview. *Essays Biochem*, 50, 1-17.

Huang D1, Gore PR, Shusta EV. (2008) Increasing yeast secretion of heterologous proteins by regulating expression rates and post-secretory loss. *Biotechnol Bioeng*. 101(6):1264-75.

Igel, M., Giesa, U., Lutjohann, D., & von Bergmann, K. (2003). Comparison of the intestinal uptake of cholesterol, plant sterols, and stanols in mice. *Journal of lipid research*, 44(3), 533–538.

Jakulj, L., van Dijk, T.H., de Boer, J.F., Kootte, R.S., Schonewille, M., Paalvast, Y. et al (2016) Transintestinal cholesterol transport is active in mice and humans and controls ezetimibe-induced fecal neutral sterol excretion. *Cell Metab*. 24, 783-794.

Johnson, B.J., Lee, J.Y., Pickert, A. and Urbatsch, I.L. (2010) Bile acids stimulate ATP hydrolysis in the purified cholesterol transporter ABCG5/G8. *Biochemistry* 49, 3403-3411.

Kamisako, T., Ogawa, H. and Yamamoto, K. (2007) Effect of cholesterol, cholic acid and cholestyramine administration on the intestinal mRNA expressions related to cholesterol and bile acid metabolism in the rat. *J. Gastroenterol. Hepatol.* 22**,** 1832-1837.

Karste K1, Bleckmann M1, van den Heuvel J2. (2017) Not Limited to E. coli: Versatile Expression Vectors for Mammalian Protein Expression. *Methods Mol Biol*. 1586:313-324.

Kidambi, S. and S.B. Patel, (2008) Sitosterolaemia: pathophysiology, clinical presentation and laboratory diagnosis. *J Clin Pathol*. 61(5): p. 588-94.

Kirchgessner, T. G., Sleph, P., Ostrowski, J., Lupisella, J., Ryan, C. S., Liu, X., Fernando, G., Grimm, D., Shipkova, P., Zhang, R., Garcia, R., Zhu, J., He, A., Malone, H., Martin, R., Behnia, K., Wang, Z., Barrett, Y. C., Garmise, R. J., Yuan, L., … Frost, R. J. (2016). Beneficial and Adverse Effects of an LXR Agonist on Human Lipid and Lipoprotein Metabolism and Circulating Neutrophils. Cell metabolism, 24(2), 223–233.

Klett, E. L., & Patel, S. (2003). Genetic defenses against noncholesterol sterols. *Current opinion in lipidology*, 14 (4), 341–345.

Klett, E. L., Lee, M. H., Adams, D. B., Chavin, K. D., & Patel, S. B. (2004). Localization of ABCG5 and ABCG8 proteins in human liver, gall bladder and intestine. *BMC gastroenterology*, 4, 21.

Krainer, F. W., Dietzsch, C., Hajek, T., Herwig, C., Spadiut, O., & Glieder, A. (2012). Recombinant protein expression in Pichia pastoris strains with an engineered methanol utilization pathway. *Microbial cell factories*, 11, 22.

Lee, J.Y., Kinch, L.N., Borek, D.M., Wang, J., Wang, J, Urbatsch, I.L. et al (2016) Crystal structure of the human sterol transporter ABCG5/ABCG8. *Nature* 533, 561-564.

Lu, K., Lee, M.H., Hazard, S., Brooks-Wilson, A., Hidaka, H., Kojima, H. et al (2001) Two genes that map to the STSL locus cause sitosterolemia: genomic structure and spectrum of mutations involving sterolin-1 and sterolin-2, encoded by ABCG5 and ABCG8, respectively. *Am. J. Hum. Genet*. 69, 278-290.

Moody, J. E., Millen, L., Binns, D., Hunt, J. F., & Thomas, P. J. (2002). Cooperative, ATP-dependent association of the nucleotide binding cassettes during the catalytic cycle of ATP-binding cassette transporters. *The Journal of biological chemistry,* 277(24), 21111–21114.

Müller D., Bayer K. and Diethard M. (2006) Potentials and limitations of prokaryotic and eukaryotic expression systems for recombinant protein production – a comparative view. *Microbial Cell Factories*, 5 (1): P6.

Nelson, R.H. (2013) Hyperlipidemia as a risk factor for cardiovascular disease. Prim. *Care* 40, 195-211.

Nguyen, T.M., Sawyer, J.K., Kelley, K.L., Davis, M.A., Kent, C.R. and Rudel, L.L. (2012) ACAT2 and ABCG5/G8 are both required for efficient cholesterol absorption in mice: evidence from thoracic lymph duct cannulation*. J. Lipid Res*. 53, 1598-1609.

Nielsen KH1. (2014) Protein expression-yeast. *Methods Enzymol*. 536:133-47.

Ohashi, R., Mu H, Wang X, Yao Q, Chen C. (2005) Reverse cholesterol transport and cholesterol efflux in atherosclerosis. *QJM*. 98(12): p. 845-56.

Ouimet, M., Barrett, T. J., & Fisher, E. A. (2019). HDL and Reverse Cholesterol Transport. *Circulation research*, 124(10), 1505–1518.

Pandey, A., Shin, K., Patterson, R. E., Liu, X. Q., & Rainey, J. K. (2016). Current strategies for protein production and purification enabling membrane protein structural biology. *Biochemistry and cell biology*, 94(6), 507–527.

Patel, S.B., Salen, G., Hidaka, H., Kwiterovich, P.O, Stalenhoef, A.F.H., Miettinen, T.A. et al (1998) Mapping a Gene Involved in Regulating Dietary Cholesterol Absorption. The Sitosterolemia Locus Is Found at Chromosome 2p21. *J. Clin. Invest.* 102, 1041-1044.

Patrick J. Loll. (2003) Membrane protein structural biology: the high throughput challenge. *Journal of Structural Biology* 142, 144–153

Phan BA, Dayspring TD, Toth PP. (2012) Ezetimibe therapy: mechanism of action and clinical update. *Vasc Health Risk Manag*. 8:415–27

Reiner Z. (2014) Resistance and intolerance to statins. *Nutr Metab Cardiovasc Dis*. 24(10):1057-1066.

Ruckenstein E., Nagarajan R. (1975) Critical micelle concentration. Transition point for micellar size distribution. *J. Phys. Chem*. 79, 24, 2622-2626.

Schoenheimer R. Z. (1929) *Physiol Chem*. 180:1.

Shuguang Pan Xiaowu Li Peng Jiang Yan Jiang Ling Shuai Yu He Zhihua Li. (2014) Variations of ABCB4 and ABCB11 genes are associated with primary intrahepatic stones. *Molecular Medicine Reports,* 11(1) p:434-446.

Simons, K., Ikonen, E. (1997) Functional rafts in cell membranes. *Nature* 387, 569 – 572.

Snapp E. (2005). Design and use of fluorescent fusion proteins in cell biology. Current protocols in cell biology, Chapter 21, 21.4.1–21.4.13.

Sumi, K., Tanaka, T., Uchida, A., Magoori, K., Urashima, Y., Ohashi, R. *et al* (2007) Cooperative Interaction between Hepatocyte Nuclear Factor 4 alpha and GATA Transcription Factors Regulates ATP-Binding Cassette Sterol Transporters ABCG5 and ABCG8. *Mol. Cell Biol.* **27,** 4248-4260.

Tall, A.R., Yvan-Charvet, L., Terasaka, N., Pagler, T., and Wang, N. (2008) HDL, ABC transporters, and cholesterol efflux: implications for the treatment of atherosclerosis. *Cell Metab*. 7(5): 365-375.

Tanapongpipat S., Promdonkoy P., Watanabe T., Tirasophon W., Roongsawang N., Chiba Y., Eurwilaichitr L. (2012) Heterologous protein expression in Pichia thermomethanolica BCC16875, a thermotolerant methylotrophic yeast and characterization of N-linked glycosylation in secreted protein. *FEMS Microbiology Letters*, 334, 2, 127–134.

Thomas and Tampé. (2018) Multifaceted structures and mechanisms of ABC transport systems in health and disease. *Curr Opin Struct Biol*, 51, 116-128.

Van der Velde, Brufau G, Groen AK. (2010) Transintestinal cholesterol efflux. *Curr Opin Lipidol* 21, 167.

Vieira Gomes, A. M., Souza Carmo, T., Silva Carvalho, L., Mendonça Bahia, F., & Parachin, N. S. (2018). Comparison of Yeasts as Hosts for Recombinant Protein Production. *Microorganisms*, 6(2), 38.

Wang, J., Einarsson, C., Murphy, C., Parini, P. Björkhem, I, Gåfvels, M. et al (2006) Studies on LXR-and FXR-mediated effects on cholesterol homeostasis in normal and cholic acid-depleted mice. *J. Lipid Res*. 47, 421–430.

Wang, J., Grishin, N., Kinch, L., Cohen, J. C., Hobbs, H. H., & Xie, X. S. (2011). Sequences in the nonconsensus nucleotide-binding domain of ABCG5/ABCG8 required for sterol transport. *The Journal of biological chemistry*, 286(9), 7308–7314.

Wang, L., Tonggu, L. (2015) Membrane protein reconstitution for functional and structural studies. *Sci. China Life Sci*. 58, 66–74

Werten, M., Eggink, G., Cohen Stuart, M. A., & de Wolf, F. A. (2019). Production of protein-based polymers in Pichia pastoris. *Biotechnology advances*, 37(5), 642–666.

Wilkens S. (2015). Structure and mechanism of ABC transporters. *F1000 prime reports*, 7, 14.

Wolfe, A. J., Si, W., Zhang, Z., Blanden, A. R., Hsueh, Y. C., Gugel, J. F., Pham, B., Chen, M., Loh, S. N., Rozovsky, S., Aksimentiev, A., & Movileanu, L. (2017). Quantification of Membrane Protein-Detergent Complex Interactions. *The journal of physical chemistry*. B, 121(44), 10228–10241.

Woodward OM, Köttgen A, and Köttgen M. (2011) ABCG transporters and disease. *FEBS J*. 278(18): 3215–3225.

Xavier, B.M., Jennings, W.J., Zein, A.A., Wang, J. and Lee, J.Y. (2019) Structural snapshot of the cholesterol-transport ATP-binding cassette proteins. Biochem. *Cell Biol*. 97, 224-233

Yang, S. T., Kreutzberger, A., Lee, J., Kiessling, V., Tamm, L. K. (2016). The role of cholesterol in membrane fusion. *Chemistry and physics of lipids*, 199, 136–143.

Yu L, Hammer RE, Li-Hawkins J, Von Bergmann K, Lutjohann D, Cohen JC, Hobbs HH. (2002) Disruption of Abcg5 and Abcg8 in mice reveals their crucial role in biliary cholesterol secretion*. Proc Natl Acad Sci USA* 99, 16237.

Yu L, von Bergmann K, Lutjohann D, Hobbs HH, Cohen JC. (2004) Selective sterol accumulation in ABCG5/ABCG8-deficient mice. *J Lipid Res.*45(2):301-307

Yu, L., Gupta, S., Xu, F., Liverman, A.D., Moschetta, A., Mangelsdorf, D.J. et al (2005) Expression of ABCG5 and ABCG8 is required for regulation of biliary cholesterol secretion. *J. Biol. Chem*. 280, 8742-8747.

Zein, A. A., Kaur, R., Hussein, T., Graf, G. A., & Lee, J. Y. (2019). ABCG5/G8: a structural view to pathophysiology of the hepatobiliary cholesterol secretion. *Biochemical Society transactions*, 47(5), 1259–1268.

Zhang, D.W., Graf, G.A., Gerard, R.D., Cohen, J.C. and Hobbs, H.H. (2006) Functional asymmetry of nucleotide-binding domains in ABCG5 and ABCG8. *J. Biol. Chem.* 281, 4507-4516.

Zoltán Hegyi and László Homolya. (2016) Functional Cooperativity between ABCG4 and ABCG1 Isoforms*. PLoS One*. 11(5): e0156516.